Journal of Computational Applied Mechanics 2021, 52(3): 507-534
DOI: 10.22059/jcamech.2021.305561.525

RESEARCH PAPER

Nonlocal effect on the axisymmetric nonlinear vibrational response of nano-disks using variational iteration method

Mojtaba Shariati [a], Mohammad Shishehsaz [1,*], Reza Mosalmani [1], Seyed Alireza Seyed Roknizadeh [1], Mohammad Hosseini [2]

[1] Department of Mechanical Engineering, Shahid Chamran University of Ahvaz, Ahvaz, Iran.
[2] Department of Mechanical Engineering, University of Hormozgan, Bandar Abbas, Iran.

Abstract
In this study, the nonlinear free vibration of a nano-disk considering small scale effects has been investigated by using the nonlocal elasticity. To take into account the nonlinear geometric effects, the nonlinear model of von Karman strain has been used while the governing differential equation was extracted according to Hamilton principle. The Galerkin weighted residual method in conjunction with the variational iteration method (VIM) was introduced to solve the governing equations for simply supported and clamped edge boundary conditions. For further comparison, the nonlinear equation was solved using the fourth-order Runge-Kutta method. Very good agreements were observed between the results of both methods, while the former method made the solution much easier. Additionally, it was observed that the ratio of thickness to radius, h/R, plays an important role on the nonlinear frequencies. This effect appears to be minute if the local elasticity theory is adopted. However, results indicated that the nonlocal effect may be ignored provided h/R ratio is very small

Keywords: Nonlinear free vibration, Nano-disks, Nonlocal elasticity Theory, Von Karman strain.

Introduction

Nano-structured elements have attracted the interest of scientific communities due to their superior properties. Conducting experiments with Nano-scale size specimens is found to be difficult and expensive. Therefore, the development of appropriate mathematical models for nanostructures is an important issue concerning their applications.

Generally, three approaches have been developed to model nanostructures. These approaches are (a) atomistic mechanics [1, 2]), (b) hybrid atomistic–continuum mechanics [3-6], and (c) continuum mechanics. Both atomistic and hybrid atomistic–continuum mechanics are computationally expensive and are not suitable for analyzing large scale systems. Continuum mechanics approach is less computationally expensive than the former two approaches. It has been found that continuum mechanics results are in good agreement with atomistic and hybrid approaches. The experimental results show that the size effects play an important role in

* Corresponding author: mshishehsaz@scu.ac.ir

mechanical properties[7, 8]; consequently, avoiding these effects may result wrong designs and unacceptable answers.

Since size effect is not considered in classical continuum theories then, these theories are not appropriate for evaluation of structures on micro and nano-levels. In nano applications, the size effects that have been experimentally observed are not interpretable by classical continuum theories due to their lack of material length scale parameters. Accordingly, size-dependent continuum theories have been developed, such as the strain gradient theory[9, 10], the modified coupled stress theory[11, 12], the nonlocal strain gradient theory[13, 14], Doublet mechanic[15, 16] and the nonlocal elasticity theory[17, 18] have been suggested. For example, the nonlinear free vibrations of single-layer orthotropic nano-plates, in a variable temperature environment was studied by Shen *et al*. [19], taking into account the assumptions of the classical theory of sheets as well as the non-local elasticity theory. In a similar study, a new model for size-dependent geometric nonlinear vibrations of Timoshenko beam based on the strain gradient theory was presented by Ramezani[20]. Additionally, the nonlinear free vibration of isotropic single-layer nano-plates was analyzed by Jomehzadeh and Saidi [21], using the non-local elasticity theory. Moreover, the nonlinear forced vibrations of the isotropic and classical nano-plates which were resting on simple supports were studied by He *et al.* [22], using the nonlocal elasticity theory. Nonlinear vibrational behavior of Kirchhoff micro-plate was studied in [23] based on the first-order gradient elasticity theory. In the study performed by Zhang *et al*.[24], the nonlinear vibrations of rectangular graphene nano-sheets were investigated. The theories of classical plates and nonlocal elasticity were used for modeling, while the numerical method of element free kp-Rits was applied to solve the nonlinear equations and extraction of the nonlinear frequencies. The nonlinear free and forced vibrational behavior of a porous functionally graded Euler-Bernoulli nano-beam subjected to mechanical and electrical loads was studied by Mohammadi *et al*. [25], using the nonlocal strain gradient elasticity theory. Moreover, other researchers have provided useful articles on nano-mechanics [17, 26-45].

One of the most important Nano-structured elements is nano-disks. These structures in size of microns and sub-microns are of practical concern in many NEMS devices like oscillators, clocks, and sensor devices as well as micro-gyroscopes[46-48]and micro-motors[49]. Also, micro-/nano-disks are employed in whispering-gallery-mode resonators [50] and photonics, due to their great potential to identify the pathogens [51]. On the other hand, one of the important photonic devices is a nano-scale refractive index sensor with a nano-disk resonator which is widely used in biosensors [52]. Additionally, scientists have attempted to control the biological activity of nano-particles, and for this reason, many researchers have carried out studies in the field of safer imaging agents for biomedical applications[53]. In this regard, they have focused on nano-disks and nano-spheres to achieve this goal[53]. Moreover, Micro-/nano-disks are commonly used in resistive switching phenomena [54], study of cell structures[55], solar cells[56, 57], nano-disk array electrodes [58-60], lasers [61-65], and sensors[66].

In spite of the vast literature on the free transverse vibration of nano-beams, nano-plates, and nano-shells, few works have been dedicated to the nonlocal elasticity study of nano-disks. The large amplitude free vibration of size-dependent circular micro-plates was studied by Wang *et al*. [67] using the modified couple stress theory. Mohammadi *et al*. [68] studied free transverse vibrational behavior of circular and annular graphene sheets (with various boundary conditions) using the nonlocal continuum plate model. Hosseini *et al*. [69] studied the stress distribution in a rotating nano-disk made of functionally graded material with nonlinearly varying thickness, based on the strain gradient theory. Based on strain gradient theory, Shishehsaz *et al*. [41] studied the thermoelastic behavior of a functionally graded nano-disk and compared their results with those of classical theory. They showed that the increase in temperature at the outside radius of the nano-disk, as well as any rise in material inhomogeneity parameter has a direct effect on the total stresses and radial displacements. In another study, Shishehsaz *et al*. [70] performed a nonlinear vibration analysis on a nano-disk, based on the nonlocal elasticity theory, in conjunction with the homotopy perturbation method. Hosseini *et al*. [71] analyzed stress distribution in a functionally graded nano-disk with variable thickness, based on strain gradient theory. The nano-disk in question was subjected to the thermal and mechanical loads while it was rotating with a constant angular velocity. They analyzed the effects of angular velocity, thickness profile, material inhomogeneity parameter, external loads and the temperature on the total stresses and radial displacements. Shishehsaz *et al*. [72] studied the effect of nonlocal parameter on the linear vibration of nano-disks based on the nonlocal elasticity theory using Adomian decomposition method. They imposed clamped and simply supported conditions on their model. Using this method, the first five axisymmetric natural frequencies and displacements of the Nano-circular plate were obtained one at a time, with enough numerical results to illustrate the influence of nonlocal parameters on the natural frequencies and displacements of the nano-circular plate. Shariati *et al*. [73] calibrated of small-scale parameters of non-classical continuum theories such as nonlocal strain gradient theory, strain gradient theory, stress-driven nonlocal elasticity, and strain-driven nonlocal elasticity. In another study, Shishehsaz *et al*.[74] investigated the vibrational behavior of a functionally graded annular nano-plate based on stress-driven model. According to their results, the material inhomogeneity index, as well as the geometry of annular plate and scale parameters have significant effects on the vibrational behavior.

Considering the subjects covered in the literature survey (and others), the main objective of this research is to investigate the axisymmetric nonlinear free vibration of a nano-disk, as well as the applicability of the powerful and efficient semi-analytical technique, namely the variational iteration method (VIM), in solving such problems. This method has shown to be effective, powerful, and very accurate, with a high rate of convergence in related calculations for solving the strongly nonlinear problems arising in other fields of micro-mechanics. The analysis will focus on the effect of nonlocal parameter, aspect ratio, different boundary conditions, and frequency number on the overall behavior of the nano-disk. For this purpose, Eringen's nonlocal elasticity theory along with Hamilton's principle will be used in conjunction with Galerkin weighted residual method to discretize the governing equation. On application of Galerkin method, the system of nonlinear differential equations (Duffing’s Equation) is obtained and hence, the natural nonlinear frequencies and mode shapes will be obtained using VIM. The deduced results will be compared with the numerical results of the fourth-order Runge–Kutta method.

Nonlocal constitutive relations

According to the nonlocal elasticity theory (Eringen's model), the stress field at point x in an elastic continuum depends not only on the strain field at that point but also on strains at all other points in the body[75]. Eringen also attributed this fact to the atomic theory of lattice dynamics and experimental observations on phonon dispersion [75]. Thus, the nonlocal stress tensor σ^{Nl} at point x is expressed as:

$$\sigma^{Nl}(x)=\int_V K\left(\left|x'-x\right|,\tau\right)\,\sigma^L(x')\,dx' \tag{1}$$

where $\sigma^L(x')$ is the macroscopic stress tensor at point x, the kernel function $K(|x'-x|,\tau)$ represents the nonlocal modulus, $|x'-x|$ is considered as the distance in Euclidean norm, and τ is a material constant that depends on the internal and external characteristic lengths (the lattice spacing and wavelength, respectively). Based on Hook's law, the macroscopic stress t at point x in a solid is related to the strain ε at that point as:

$$t(x)=C(x):\varepsilon(x) \tag{2}$$

where C is the fourth-order elasticity tensor and: indicates the double-dot product.

The constitutive Eq. (1) and (2), define the nonlocal constitutive behavior of a solid based on Hook's law. Equation (1) represents the weighted average of the strain field contributions from all other points in the body to the stress field at a point in question. However, the integral constitutive relation in Eq. (1) makes the elasticity problems difficult to solve. It has been shown that it is possible to present the integral constitutive relations in an equivalent differential form as [75]:

$$\left(1-(e_0a)^2\nabla^2\right)\sigma^{Nl}=\sigma^L \tag{3}$$

where e_0 and a are the material constant and the internal characteristic lengths, respectively. Moreover, the Laplace operator ∇^2 in the polar coordinates is defined as[76]:

$$\nabla^2=\frac{\partial^2}{\partial r^2}+\frac{1}{r}\frac{\partial}{\partial r}+\frac{1}{r^2}\frac{\partial^2}{\partial\theta^2} \tag{4}$$

Problem formulation

Figure 1 shows a linearly elastic homogeneous isotropic nano-plate with a circular cross-section of R and thickness h. To derive the governing equations, a cylindrical coordinate system (r, θ, z) is attached to the plate where its surface lies in r-θplane. According to Kirchhoff's kinematics of thin plates, the displacement components of the plate, namely u_r, u_θ, and u_z are expressed by Eq. (5) [77, 78]:

$$u_r(r,\theta,z,t)=u(r,\theta,t)-z\frac{\partial w}{\partial r}(r,\theta,t),\quad u_\theta(r,\theta,z,t)=v(r,\theta,t)-\frac{z}{r}\frac{\partial w}{\partial r}(r,\theta,t),$$
$$u_z(r,\theta,z,t)=w(r,\theta,t). \tag{5}$$

where u, v, and w are the radial, tangential, and transverse displacements of the plate middle surface, respectively.

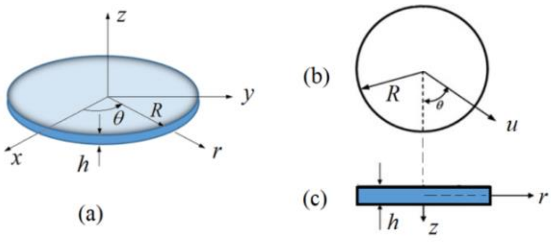

Figure 1. Main features of the plate geometry, (a) nano-disk, (b) top view, and (c) side view.

Now, the von Kármán nonlinear strain-displacement relationships are written as [77, 78]:

$$\varepsilon_{rr}=\frac{\partial u_r}{\partial r}+\frac{1}{2}\left(\frac{\partial u_z}{\partial r}\right)^2,\quad \varepsilon_{\theta\theta}=\frac{u_r}{r}+\frac{1}{r}\frac{\partial u_\theta}{\partial\theta}+\frac{1}{2}\left(\frac{1}{r}\frac{\partial u_z}{\partial\theta}\right)^2,$$
$$\gamma_{r\theta}=\frac{1}{r}\left(\frac{\partial u_r}{\partial\theta}-u_\theta\right)+\frac{\partial u_\theta}{\partial r}+\frac{1}{r}\frac{\partial u_z}{\partial r}\frac{\partial u_z}{\partial\theta}. \tag{6}$$

These equations are written based on the local shear stress-strain constitutive relation.

Substituting the displacement fields, Eq. (5), into Eq. (6) gives:

$$\varepsilon_{rr}=\frac{\partial u}{\partial r}+\frac{1}{2}\left(\frac{\partial w}{\partial r}\right)^2-z\frac{\partial^2 w}{\partial r^2},$$
$$\varepsilon_{\theta\theta}=\frac{u}{r}+\frac{1}{r}\frac{\partial v}{\partial\theta}+\frac{1}{2r^2}\left(\frac{\partial w}{\partial\theta}\right)^2-\frac{z}{r}\left(\frac{\partial w}{\partial r}+\frac{1}{r}\frac{\partial^2 w}{\partial\theta^2}\right), \tag{7}$$
$$\gamma_{r\theta}=\frac{1}{r}\frac{\partial u}{\partial\theta}+\frac{\partial v}{\partial r}-\frac{v}{r}+\frac{1}{r}\frac{\partial w}{\partial r}\frac{\partial w}{\partial\theta}-z\frac{2}{r}\left(\frac{\partial^2 w}{\partial r\partial\theta}-\frac{1}{r}\frac{\partial w}{\partial\theta}\right).$$

Using Hamilton's principle, the equations of motion can be obtained as [77, 78]:

$$\frac{1}{r}\left(\frac{\partial}{\partial r}(rN_{rr})+\frac{\partial N_{r\theta}}{\partial r}-N_{\theta\theta}\right)-I_0\frac{\partial^2 u}{\partial t^2}=0,\qquad \frac{1}{r}\left(\frac{\partial}{\partial r}(rN_{r\theta})+\frac{\partial N_{\theta\theta}}{\partial\theta}+N_{r\theta}\right)-I_0\frac{\partial^2 v}{\partial t^2}=0,$$
$$\frac{1}{r}\left\{\frac{\partial^2}{\partial r^2}(rM_{rr})-\frac{\partial M_{\theta\theta}}{\partial r}+\frac{1}{r}\frac{\partial^2 M_{\theta\theta}}{\partial\theta^2}+2\frac{\partial^2 M_{r\theta}}{\partial r\partial\theta}+\frac{1}{r}\frac{\partial M_{r\theta}}{\partial\theta}+\frac{\partial}{\partial r}\left(rN_{rr}\frac{\partial w}{\partial r}\right)+\frac{1}{r}\frac{\partial}{\partial r}\left(N_{\theta\theta}\frac{\partial w}{\partial\theta}\right)\right\} \tag{8}$$
$$-I_0\frac{\partial^2 w}{\partial t^2}+I_2\frac{\partial^2}{\partial t^2}\left(\frac{1}{r}\frac{\partial}{\partial r}\left(r\frac{\partial w}{\partial r}\right)+\frac{1}{r^2}\frac{\partial^2 w}{\partial\theta^2}\right)=0.$$

In the above equations, I_0 is the mass moment of inertia and I_2 is the rotary inertia of the nano-disk. These two parameters are defined as:

$$(I_0,I_2)=\int_{-h/2}^{+h/2}\rho\left(1,z^2\right)dz=\left(\rho h\,,\ \frac{1}{12}\rho h^3\right) \tag{9}$$

In Eq. (9) ρ and h are the density and thickness of the nano-plate respectively.

On using Eq. (3), based on the nonlocal elasticity, the plane stress constitutive relations for the plate are:

$$\left(1-(e_0a)^2\nabla^2\right)\sigma_{rr}=\frac{E}{1-\upsilon^2}(\varepsilon_{rr}+\upsilon\varepsilon_{\theta\theta}),\quad \left(1-(e_0a)^2\nabla^2\right)\sigma_{\theta\theta}=\frac{E}{1-\upsilon^2}(\upsilon\varepsilon_{rr}+\varepsilon_{\theta\theta}),$$
$$\left(1-(e_0a)^2\nabla^2\right)\tau_{r\theta}=2G\varepsilon_{r\theta}. \tag{10}$$

where υ is Poisson's ratio [79].

Moreover, to obtain the governing equations, the following stress resultants are used in formulations yet to come.

$$\left(N_{rr}\ ,\ N_{\theta\theta},N_{r\theta}\right)=\int_{-\frac{h}{2}}^{+\frac{h}{2}}\left(\sigma_{rr}\ ,\ \sigma_{\theta\theta},\ \tau_{r\theta}\right)dz,$$
$$\left(M_{rr}\ ,\ M_{\theta\theta},M_{r\theta}\right)=\int_{-\frac{h}{2}}^{+\frac{h}{2}}\left(\sigma_{rr}\ ,\ \sigma_{\theta\theta},\ \tau_{r\theta}\right)zdz. \tag{11}$$

For a homogeneous isotropic nano-plate, based on the strain displacement relation, Eq. (7), as well as the stress resultants defined in Eq. (11), the stress-strain relations, Eq. (10), are recast as:

$$\left(1-\left(e_0a\right)^2\nabla^2\right)M_{rr}=-D\left\{\frac{\partial^2 w}{\partial r^2}+\frac{\upsilon}{r}\left(\frac{\partial w}{\partial r}+\frac{1}{r}\frac{\partial^2 w}{\partial\theta^2}\right)\right\},$$
$$\left(1-\left(e_0a\right)^2\nabla^2\right)M_{\theta\theta}=-D\left\{\upsilon\frac{\partial^2 w}{\partial r^2}+\frac{1}{r}\left(\frac{\partial w}{\partial r}+\frac{1}{r}\frac{\partial^2 w}{\partial\theta^2}\right)\right\}, \tag{11}$$
$$\left(1-\left(e_0a\right)^2\nabla^2\right)M_{r\theta}=-\left(1-\upsilon\right)D\frac{1}{r}\left(\frac{\partial^2 w}{\partial r\partial\theta}-\frac{1}{r}\frac{\partial w}{\partial\theta}\right).$$

where $D = Eh^3/12(1-\nu^2)$ represents the flexural rigidity[79].

When the in-plane natural frequencies are large compared with the transverse natural frequencies, then the in-plane inertia term can be neglected and first and second equations of Eq. (8) are recast as [80]:

$$\frac{\partial}{\partial r}\left(rN_{rr}\right)+\frac{\partial N_{r\theta}}{\partial r}-N_{\theta\theta}=0,\quad \frac{\partial}{\partial r}\left(rN_{r\theta}\right)+\frac{\partial N_{\theta\theta}}{\partial\theta}+N_{r\theta}=0. \tag{13}$$

Now, the stress function F (sometimes referred as the stress Airy function) is defined as:

$$N_{rr}=\frac{1}{r}\frac{\partial F}{\partial r}+\frac{1}{r^2}\frac{\partial^2 F}{\partial\theta^2},\qquad N_{\theta\theta}=\frac{\partial^2 F}{\partial r^2},$$
$$N_{r\theta}=\frac{1}{r^2}\frac{\partial F}{\partial\theta}-\frac{1}{r}\frac{\partial^2 F}{\partial r\partial\theta}. \tag{14}$$

such that it satisfies Eq.(13)[80].

In axisymmetric loading, since $\partial/\partial\theta = 0$, then thied equation of Eq.(8) is rewritten in the following form:

$$\frac{1}{r}\left\{\frac{\partial^2}{\partial r^2}\left(rM_{rr}\right)-\frac{\partial M_{\theta\theta}}{\partial r}\right\}+\frac{1}{r}\frac{\partial}{\partial r}\left(rN_{rr}\frac{\partial w}{\partial r}\right)-I_0\frac{\partial^2 w}{\partial t^2}+I_2\frac{\partial^2}{\partial t^2}\left(\frac{1}{r}\frac{\partial}{\partial r}\left(r\frac{\partial w}{\partial r}\right)\right)=0 \tag{15}$$

Substituting the axisymmetric form of Eq. (12) into Eq. (15), then the equation of motion is obtained as:

$$D\nabla^4 w+\left(1-(e_0a)^2\nabla^2\right)\left\{I_0\frac{\partial^2}{\partial t^2}w-\frac{I_2}{r}\left(\frac{\partial}{\partial r}\frac{\partial^2}{\partial t^2}w+\frac{\partial^2}{\partial r^2}\frac{\partial^2}{\partial t^2}w\right)-\frac{1}{r}\frac{\partial}{\partial r}\left(\frac{\partial F}{\partial r}\frac{\partial w}{\partial r}\right)\right\}=0 \tag{16}$$

Here, the operator ∇^4, defined in polar coordinates, is equal to [76]:

$$\nabla^4=\frac{\partial^4}{\partial r^4}+\frac{2}{r}\frac{\partial^3}{\partial r^3}-\frac{1}{r^2}\frac{\partial^2}{\partial r^2}+\frac{1}{r^3}\frac{\partial}{\partial r}+\frac{2}{r^2}\frac{\partial^4}{\partial r^2\partial\theta^2}-\frac{2}{r^3}\frac{\partial^3}{\partial r\partial\theta^2}+\frac{4}{r^4}\frac{\partial^2}{\partial\theta^2}+\frac{1}{r^4}\frac{\partial^4}{\partial\theta^4} \tag{17}$$

In the axisymmetric case, the differential operator ∇^2 and ∇^4 are given by:

$$\nabla^2=\frac{\partial^2}{\partial r^2}+\frac{1}{r}\frac{\partial}{\partial r},\qquad \nabla^4=\frac{\partial^4}{\partial r^4}+\frac{2}{r}\frac{\partial^3}{\partial r^3}-\frac{1}{r^2}\frac{\partial^2}{\partial r^2}+\frac{1}{r^3}\frac{\partial}{\partial r}\ . \tag{18}$$

Using Eq. (10) and (11), the governing relations between stress resultants and strain components can be written as:

$$\left(1-(e_0a)^2\nabla^2\right)N_{rr}=\frac{Eh}{1-\upsilon^2}(\varepsilon_{rr}+\upsilon\varepsilon_{\theta\theta}),\quad \left(1-(e_0a)^2\nabla^2\right)N_{\theta\theta}=\frac{Eh}{1-\upsilon^2}(\upsilon\varepsilon_{rr}+\varepsilon_{\theta\theta}). \tag{19}$$

For the case of axisymmetric loading, Eq. (14), (7) are reduced to:

$$N_{rr}=\frac{1}{r}\frac{\partial F}{\partial r},\quad N_{\theta\theta}=\frac{\partial^2 F}{\partial r^2},\quad \varepsilon_{rr}=\frac{\partial u}{\partial r}+\frac{1}{2}\left(\frac{\partial w}{\partial r}\right)^2,\quad \varepsilon_{\theta\theta}=\frac{u}{r}. \tag{20}$$

Similarly, Eq. (19) are:

$$\begin{aligned}&\left(1-(e_0a)^2\nabla^2\right)\left(\frac{1}{r}\frac{\partial F}{\partial r}\right)=\frac{Eh}{1-\upsilon^2}\left\{\frac{\partial u}{\partial r}+\frac{1}{2}\left(\frac{\partial w}{\partial r}\right)^2+\upsilon\frac{u}{r}\right\},\\&\left(1-(e_0a)^2\nabla^2\right)\frac{\partial^2 F}{\partial r^2}=\frac{Eh}{1-\upsilon^2}\left\{\frac{u}{r}+\upsilon\left(\frac{\partial u}{\partial r}+\frac{1}{2}\left(\frac{\partial w}{\partial r}\right)^2\right)\right\}.\end{aligned} \tag{21}$$

Eliminating u from Eq. (21a) and (21b), the compatibility equation is obtained as:

$$\left(1-(e_0a)^2\nabla^2\right)\left\{r\frac{\partial^3 F}{\partial r^3}+\frac{\partial^2 F}{\partial r^2}-\frac{1}{r}\frac{\partial F}{\partial r}\right\}+\frac{1}{2}Eh\left(\frac{\partial w}{\partial r}\right)^2=0 \tag{22}$$

Equation (22) can be recast as follows:

$$\left(1-(e_0a)^2\nabla^2\right)\nabla^4 F+\frac{Eh}{r}\left(\frac{\partial^2 w}{\partial r^2}\frac{\partial w}{\partial r}\right)=0 \tag{23}$$

Finally, the equation of motion and compatibility equation for the nano-disk are:

$$D\nabla^4 w+\left(1-(e_0a)^2\nabla^2\right)\left\{I_0\frac{\partial^2}{\partial t^2}w-\frac{I_2}{r}\frac{\partial}{\partial r}\left(r\frac{\partial}{\partial r}\frac{\partial^2}{\partial t^2}w\right)-\frac{1}{r}\frac{\partial}{\partial r}\left(\frac{\partial F}{\partial r}\frac{\partial w}{\partial r}\right)\right\}=0,$$
$$\left(1-(e_0a)^2\nabla^2\right)\nabla^4 F+\frac{Eh}{r}\left(\frac{\partial^2 w}{\partial r^2}\frac{\partial w}{\partial r}\right)=0. \tag{24}$$

These equations are the governing differential equations for large deflections of a nano-disk, based on an axisymmetric loading condition. Determination of the transverse displacement $w(r,t)$ and the stress function $F(r,t)$ requires the solution of these equations, which must, of course, satisfy the boundary conditions. The boundary conditions for simply supported and clamped edge constraints at r = $R$are as follows respectively [81]:

$$\text{(a):}\frac{\partial F}{\partial r}=0,\qquad w=0,\quad M_{rr}=0$$
$$\text{(b):}\frac{\partial^2 F}{\partial r^2}-\frac{\upsilon}{r}\frac{\partial F}{\partial r}=0,\quad w=0,\quad \frac{\partial w}{\partial r}=0 \tag{25}$$

Denoting the non-dimensional variables by asterisks (except for μ), They can be written as:

$$r=Rr^*\ ,\ t=R^2\sqrt{\frac{\rho h}{D}}\,t^*,\quad w=\frac{h^2}{R}w^*\ ,\ F=\frac{Eh^5}{R^2}F^*,\quad \frac{e_0a}{R}=\mu. \tag{26}$$

Substituting Eq. (26) into Eqs. (24), while using Eq. (8), the non-dimensional governing equations

$$\nabla^4 w^*+\left(1-\mu^2\nabla^2\right)\left\{\frac{\partial^2}{\partial t^2}w^*-\frac{h^2}{12R^2}\frac{1}{r^*}\frac{\partial}{\partial r^*}\left(r^*\frac{\partial}{\partial r^*}\frac{\partial^2}{\partial t^2}w^*\right)\right.$$
$$\left.-\frac{12\left(1-\upsilon^2\right)h^2}{R^2}\frac{1}{r^*}\frac{\partial}{\partial r^*}\left(\frac{\partial w^*}{\partial r^*}\frac{\partial F^*}{\partial r^*}\right)\right\}=0 \tag{27}$$

$$\left(1-\mu^2\nabla^2\right)\nabla^4 F^*+\frac{1}{r^*}\left(\frac{\partial^2 w^*}{\partial r^{*2}}\frac{\partial w^*}{\partial r^*}\right)=0 \tag{28}$$

and the boundary conditions for simply supported and clamped edge constraints at $r^*=1$ are as follows respectively:

$$\text{(a):}\frac{\partial F^*}{\partial r^*}=0,\quad w^*=0,\quad M_{r^*r^*}=0,$$
$$\text{(b):}\frac{\partial^2 F^*}{\partial r^{*2}}-\frac{\upsilon}{r^*}\frac{\partial F^*}{\partial r^*}=0,\quad w^*=0,\quad \frac{\partial w^*}{\partial r^*}=0. \tag{29}$$

Solution procedure

Galerkin weighted residual Method

Equations (27) and (28) are the consistent basic relations for the nano-disk model. These equations that are derived based on the nonlocal elasticity theory represent the strong forms of the governing equations and are reduced into the equations of a circular plate provided μ=0. Owing to the fact that finding the exact solution from these equations is commonly difficult, then a weak form of these equations is usually generated for any further process. Here, the Galerkin weighted residual method, as a general mathematical tool, is used to create the weak forms of the foregoing equations. According to this approach, the nonlinear free vibration response of the nano-disk can be obtained by introducing the following admissible functions for $F^*$and the non-dimensional transverse deflection w^*.

$$w^*\left(r^*,t^*\right)=\sum_{i=1}^{m}\varphi_i\left(r^*\right)q_i\left(t^*\right),\quad F^*\left(r^*,t^*\right)=\sum_{i=1}^{m}\varphi_i\left(r^*\right)\tilde{q}_i\left(t^*\right)+f\left(r^*\right). \tag{30}$$

In Eq. (30), m is the number of half-waves in r direction, $\varphi_i\left(r^*\right)$ are the known basic functions that must satisfy the boundary conditions of the nano-disk, $q_i\left(t^*\right)$, and $\tilde{q}_i\left(t^*\right)$ are the time variant-coefficient of the mode shape functions, and $f(r^*)$ is the homogeneous solution to Eq. (27) which is equal to;

$$f\left(r^*\right)=A_1\frac{1}{2}r^{*2}+A_2\,ln\,r^*+A_3 \tag{31}$$

The integral constants A_1, A_2, and A_3 should be determined by the use of boundary conditions. If the transverse deflection at the center of the plate is not to be infinitely large, then A_2 must be equal to zero; and hence, based on the boundary conditions given as Eq. (29), the value of A_3 becomes unimportant. As a result, Eq. (30) become:

$$w\left(r^*,t^*\right)=\sum_{i=1}^{m}\varphi_i\left(r^*\right)q_i\left(t^*\right),\quad F^*\left(r^*,t^*\right)=\sum_{i=1}^{m}\psi_i\left(r^*\right)\tilde{q}_i\left(t^*\right). \tag{32}$$

where $\psi_i(r^*)$ for simply supported and clamped edge are defined such as:

$$\psi_i\left(r^*\right)=\varphi_i\left(r^*\right)-\frac{1}{2}r^{*2}\varphi_i'(1),\quad \psi_i\left(r^*\right)=\varphi_i\left(r^*\right)-\frac{r^{*2}}{2(1-\upsilon)}\left\{\varphi_i''(1)-\upsilon\varphi_i'(1)\right\}. \tag{33}$$

On using Eq. (32) in conjunction with the Galerkin method, Eq. (28) can be rewritten in the following form:

$$\begin{aligned}&\int_0^1\psi_i\left(r^*\right)\left\{\sum_{j=1}^{m}\left(1-\mu^2\nabla^2\right)\nabla^4\psi_j\left(r^*\right)\tilde{q}_j\left(t^*\right)\right.\\&\left.+\frac{1}{r^*}\sum_{j=1}^{m}\left(\frac{d^2\varphi_j\left(r^*\right)}{dr^{*2}}\right)q_j\left(t^*\right)\sum_{k=1}^{m}\left(\frac{d\varphi_k\left(r^*\right)}{dr^*}\right)q_k\left(t^*\right)\right\}dr^*=0\qquad(i=1,...,m)\end{aligned} \tag{34}$$

The solution to Eq. (34) can be expressed as;

$$\sum_{j=1}^{m}\alpha_{ij}\tilde{q}_j\left(t^*\right)=\sum_{j=1}^{m}\sum_{k=1}^{m}\beta_{ijk}q_j\left(t^*\right)q_k\left(t^*\right)\quad\left(i=1,...,m\right)\tag{35}$$

where,

$$\alpha_{ij}=\int_0^1\psi_i\left(r^*\right)\left(1-\mu^2\nabla^2\right)\nabla^4\psi_j\left(r^*\right)dr^*,\quad \beta_{ijk}=-\int_0^1\frac{1}{r^*}\psi_i\left(r^*\right)\left(\frac{d\varphi_j\left(r^*\right)}{dr^*}\right)\left(\frac{d^2\varphi_k\left(r^*\right)}{dr^{*2}}\right)dr^*.\tag{36}$$

Solving Eq. (35) for the time variant-coefficient of the mode shape functions $\tilde{q}_i\left(t^*\right)$, one can write;

$$\tilde{q}_i\left(t^*\right)=\sum_{j=1}^{m}\sum_{k=1}^{m}\gamma_{ijk}q_j\left(t^*\right)q_k\left(t^*\right)\quad\left(i=1,...,m\right)\tag{37}$$

Substituting Eq. (37) back into Eq. (32) and applying the Galerkin method to Eq. (27) while using Eq. (33), Eq. (32) can be obtained in the following form:

$$\sum_{j=1}^{m}M_{ij}\frac{d^2}{dt^2}q_j\left(t^*\right)+\sum_{j=1}^{m}K_{ij}q_j\left(t^*\right)+\sum_{j=1}^{m}\sum_{k=1}^{m}\sum_{r=1}^{m}\sum_{s=1}^{m}H_{ijkrs}\,q_k\left(t^*\right)q_r\left(t^*\right)q_s\left(t^*\right)=0\ ,\left(i=1,...,m\right)\tag{38}$$

in which,

$$\begin{aligned}
M_{ij}&=\int_0^1\varphi_i\left(r^*\right)\left\{\left(1-\mu^2\nabla^2\right)\right\}\times\left\{\varphi_j\left(r^*\right)-\frac{h^2}{12R^2}\frac{1}{r^*}\frac{d}{dr^*}\left(r^*\frac{d}{dr^*}\varphi_j\left(r^*\right)\right)\right\}dr^*,\\
K_{ij}&=\int_0^1\varphi_i\left(r^*\right)\nabla^4\varphi_j\left(r^*\right)dr^*,\\
H_{ijkrs}&=-12\left(1-\upsilon^2\right)\frac{h^2}{R^2}\gamma_{jkr}\int_0^1\varphi_i\left(r^*\right)\left(1-\mu^2\nabla^2\right)\times\left\{\frac{1}{r^*}\frac{d}{dr^*}\left(\frac{d\psi_j\left(r^*\right)}{dr^*}\frac{d\varphi_s\left(r^*\right)}{dr^*}\right)\right\}dr^*
\end{aligned}\tag{39}$$

For linear vibration of the nano-disk, the nonlinear term in Eq. (38) can be neglected. The corresponding linear frequencies are then given by the eigenvalues of the matrix product $\boldsymbol{M}^{-1}\boldsymbol{K}$, where $\boldsymbol{M}$ and $\boldsymbol{K}$ are the mass and stiffness matrices of the linear system that are defined as;

$$\boldsymbol{M}=\left[M_{ij}\right]\quad,\quad\boldsymbol{K}=\left[K_{ij}\right].\tag{40}$$

Equation (38) (Duffing equation), has received numerous attentions in recent decades due to a variety of engineering applications. Surveying the literature shows that a variety of solution methods have been developed so far to solve this equation.

The Variational Iteration Method

Variational iteration method (VIM), which is currently used by many researchers, is able to solve a large class of nonlinear ordinary differential equations. The flexibility and adaptability provided by this method make it easily applicable to different classes of problems in applied and engineering sciences [82-85]. VIM has been favorably applied to various kinds of nonlinear problems; for example, fractional differential equations[86, 87], nonlinear differential equations[88], nonlinear thermo-elasticity[89], and nonlinear wave equations[90, 91]. To illustrate the method, consider the following general functional equation.

$$Lq(r)+N(r)=g(r) \tag{41}$$

Where L is a linear operator, N is a non-linear operator and $g(r)$ is a known analytical function. According to the VIM, the following correction functional can be constructed such that [82-85]:

$$q_{n+1}(r)=q_n(r)+\int_0^r \lambda(\xi)\left\{Lq_n(\xi)+N\tilde{q}_n(\xi)-g(\xi)\right\}d\xi\ , \quad n\geq 0 \tag{42}$$

Here, the subscript n denotes the n^{th} approximation, λ is a general Lagrange multiplier and the second term on the right side of Eq. (42) is called the correction term [92]. Moreover, $\tilde{q}_n$ is considered as the restricted variation and $\delta\tilde{q}_n=0$ [93, 94]. The Lagrange multiplier λ can be identified optimally via the variational theory[94]. The successive approximations $q_{n+1}(r)$ of the solution $q(r)$ will be readily obtained upon using the obtained Lagrange multiplier and by using any selective function $q_0(r)$. Consequently, the exact solution can be obtained via Eq. (43).

$$q(r)=\lim_{n\to\infty} q_n(r) \tag{43}$$

when $q_n(r)$ has a limit as $n\to\infty$ [94].

To solve Eq. (38) by means of VIM, the arbitrary initial approximation is chosen as:

$$q_{i,0}\left(t^*\right)=q_{i,0}\cos\left(\Omega_{Nl,i}t^*\right) \qquad (i=1,\ldots,m) \tag{44}$$

Where $\Omega_{Nl,i}$ is the i^{th} nonlinear dimensionless frequency of the nano-disk and m is the number of half-waves in r direction. From Eq. (38), we have:

$$\begin{aligned}\sum_{j=1}^{m} M_{ij}\frac{d^2}{dt^2}q_j &= -\sum_{j=1}^{m}K_{ij}q_{j,0}\cos\left(\Omega_{Nl,j}t^*\right)\\ &-\sum_{j=1}^{m}\sum_{r=1}^{m}\sum_{s=1}^{m}H_{ijrs}\, q_{j,0}q_{r,0}q_{s,0}\cos^3\left(\Omega_{Nl,j}t^*\right)=0\ , \quad (i=1,\ldots,m)\end{aligned} \tag{45}$$

Equation (45) can is recast as follows:

$$\sum_{j=1}^{m} M_{ij}\frac{d^2}{dt^2}q_j = -\sum_{j=1}^{m} K_{ij}q_{j,0}\cos\left(\Omega_{Nl,j}t^*\right) - \frac{3}{4}\sum_{j=1}^{m}\sum_{r=1}^{m}\sum_{s=1}^{m} H_{ijsk}q_{j,0}q_{r,0}q_{s,0}\cos\left(\Omega_{Nl,j}t^*\right) - \frac{1}{4}\sum_{j=1}^{m}\sum_{r=1}^{m}\sum_{s=1}^{m} H_{ijsk}q_{j,0}q_{r,0}q_{s,0}\cos\left(3\Omega_{Nl,j}t^*\right), \quad (i=1,...,m) \tag{46}$$

Integrating Eq. (46) twice with respect to t^*, yields:

$$\sum_{j=1}^{m} M_{ij}q_j = \frac{1}{\Omega_{Nl,j}^2}\sum_{j=1}^{m} K_{ij}q_{j,0}\cos\left(\Omega_{Nl,j}t^*\right) + \frac{3}{4}\frac{1}{\Omega_{Nl,j}^2}\sum_{j=1}^{m}\sum_{r=1}^{m}\sum_{s=1}^{m} H_{ijsk}q_{j,0}q_{r,0}q_{s,0}\cos\left(\Omega_{Nl,j}t^*\right) + \frac{1}{36}\frac{1}{\Omega_{Nl,j}^2}\sum_{j=1}^{m}\sum_{r=1}^{m}\sum_{s=1}^{m} H_{ijsk}q_{j,0}q_{r,0}q_{s,0}\cos\left(3\Omega_{Nl,j}t^*\right), \quad (i=1,...,m) \tag{47}$$

Neglecting the coefficients of $\cos\left(3\Omega_{Nl,j}t^*\right)$ in the Eq. (47), the following nonlinear system is obtained:

$$\sum_{j=1}^{m} M_{ij}q_j = \frac{1}{\Omega_{Nl,j}^2}\sum_{j=1}^{m} K_{ij}q_{j,0}\cos\left(\Omega_{Nl,j}t^*\right) + \frac{3}{4}\frac{1}{\Omega_{Nl,j}^2}\sum_{j=1}^{m}\sum_{r=1}^{m}\sum_{s=1}^{m} H_{ijsk}q_{j,0}q_{r,0}q_{s,0}\cos\left(\Omega_{Nl,j}t^*\right) \quad (i=1,..,m) \tag{48}$$

Equation(48) can be easily solved by using a simple mathematical algorithm such as Newton-Raphson technique[95]where the results can be displayed as:

$$q_i\left(t^*\right) = f\left(\Omega_{Nl,j}, M_{ij}, K_{ij}, H_{ijsk}, q_{0,j}\right)\cos\left(\Omega_{Nl,i}t^*\right) \qquad (i,j=1,...,m) \tag{49}$$

Equating the coefficients of $\cos\left(\Omega_{Nl,j}t^*\right)$ in Eq. (44) and (49), gives the following result:

$$q_{i,0} = f_i\left(\Omega_{Nl,j}, M_{ij}, K_{ij}, H_{ijsk}, q_{0,j}\right) \qquad (i,j=1,...,m) \tag{50}$$

Consequently, the nonlinear frequencies $\Omega_{Nl,i}$ can be obtained from the Eq. (50).

According to Eq. (41) and (42), the correction functional of Eq. (38) can be constructed as follows:

$$q_{i,n+1}\left(t^*\right)=q_{i,n}\left(t^*\right)+\int_0^{t^*}\lambda_i\left(\xi\right)\left\{M_{ii}\frac{d^2}{dt^2}q_{j,n}\left(\xi\right)+K_{ii}q_{j,n}\left(\xi\right)\right.$$
$$+\sum_{\substack{j=1\\ j\neq i}}^{n}M_{ij}\frac{d^2}{dt^2}q_{j,n}\left(\xi\right)+\sum_{\substack{j=1\\ j\neq i}}^{n}K_{ij}\tilde{q}_{j,n}\left(\xi\right) \tag{51}$$
$$\left.+\sum_{j=1}^{n}\sum_{r=1}^{n}\sum_{s=1}^{n}H_{ijrs}\,\tilde{q}_{j,n}\left(\xi\right)\tilde{q}_{r,n}\left(\xi\right)\tilde{q}_{s,n}\left(\xi\right)\right\}d\xi$$
$$\left(i=1,\dots,m\right),\left(n\geq 0\right)$$

Now taking the variation of Eq. (51) with respect to the independent variable q_n and observing the fact that $\tilde{q}_{i,n}$ is a restricted variation ($\delta N\tilde{q}_n=0$) and $\delta q_i\left(0\right)=0$,then the result can be written in the following form:

$$\delta q_{i,n+1}\left(t^*\right)=\delta q_{i,n}\left(t^*\right)+\int_0^{t^*}\lambda_i\left(\xi\right)\left\{M_{ii}\delta\ddot{q}_{j,n}\left(\xi\right)+K_{ii}\delta q_{j,n}\left(\xi\right)\right\}d\xi=0,\ \left(i=1,\dots,m\right) \tag{52}$$

Obviously, the stationary conditions of Eq. (52) can be obtained as follows:

$$1-\lambda'\big|_{\xi=t}=0,\quad \lambda\big|_{\xi=t}=0,\quad \lambda''+\frac{K_{ii}}{M_{ii}}\lambda=0,\qquad \left(i=1,\dots,m\right). \tag{53}$$

Therefore, the λ_i multiplier can be identified as:

$$\lambda_i=\sqrt{\frac{M_{ii}}{K_{ii}+G_{ii}}}\,sin\sqrt{\frac{K_{ii}+G_{ii}}{M_{ii}}}\left(\xi-t\right)\qquad \left(i=1,\dots,m\right) \tag{54}$$

As a result, the iteration formula is obtained as follows:

$$q_{i,n+1}\left(t^*\right)=q_{i,n}\left(t^*\right)+\int_0^{t^*}\sqrt{\frac{M_{ii}}{K_{ii}+G_{ii}}}\,sin\sqrt{\frac{K_{ii}+G_{ii}}{M_{ii}}}\left(\xi-t\right)$$
$$\times\left\{M_{ii}\frac{d^2}{dt^2}q_{j,n}\left(\xi\right)+K_{ii}q_{j,n}\left(\xi\right)+\sum_{\substack{j=1\\ j\neq i}}^{n}M_{ij}\frac{d^2}{dt^2}\tilde{q}_{j,n}\left(\xi\right)\right. \tag{55}$$
$$\left.+\sum_{\substack{j=1\\ j\neq i}}^{n}K_{ij}\tilde{q}_{j,n}\left(\xi\right)+\sum_{j=1}^{n}\sum_{r=1}^{n}\sum_{s=1}^{n}H_{ijrs}\,\tilde{q}_{j,n}\left(\xi\right)\tilde{q}_{r,n}\left(\xi\right)\tilde{q}_{s,n}\left(\xi\right)\right\}d\xi$$
$$\left(i=1,\dots,m\right)$$

According to the iteration formula (Eq. (55)), the time-dependent coefficients $q_i(t^*)$ of the mode shape functions can be directly obtained. Then, on using Eq. (56), one can obtain the exact solution when $q_{i,n}(t^*)$has a limit as $n\to\infty$[94].

$$q_i\left(t^*\right)=\lim_{n\to\infty} q_{i,n}\left(t^*\right) \tag{56}$$

Based on the results in [96], the operator $A_i\left(q_1,q_2,...q_m\right)$ is defined as:

$$\begin{aligned}
A_i\left(q_1,q_2,...q_m\right)=&\int_0^{t^*}\sqrt{\frac{M_{ii}}{K_{ii}+G_{ii}}}\sin\sqrt{\frac{K_{ii}+G_{ii}}{M_{ii}}}\left(\xi-t\right)\\
&\times\left\{M_{ii}\frac{d^2}{dt^2}q_j\left(\xi\right)+K_{ii}q_j\left(\xi\right)+\sum_{\substack{j=1\\ j\neq i}}^{n}M_{ij}\frac{d^2}{dt^2}\tilde{q}_j\left(\xi\right)\right.\\
&\left.+\sum_{\substack{j=1\\ j\neq i}}^{n}K_{ij}\tilde{q}_j\left(\xi\right)+\sum_{j=1}^{n}\sum_{r=1}^{n}\sum_{s=1}^{n}H_{ijrs}\,\tilde{q}_j\left(\xi\right)\tilde{q}_r\left(\xi\right)\tilde{q}_s\left(\xi\right)\right\}d\xi,\left(i=1,...,m\right)
\end{aligned} \tag{57}$$

While the components $d_{i,n}\left(t^*\right),\left(n=1,2,...\right)$, are defined such that:

$$\begin{aligned}
&d_{i,0}\left(t^*\right)=q_{i,0}\ ,\ d_{i,1}\left(t^*\right)=A_i\left(d_{i,0}\left(t^*\right)\right),\ \ d_{i,2}\left(t^*\right)=A_i\left(d_{i,0}\left(t^*\right)+d_{i,1}\left(t^*\right)\right),\\
&\vdots\\
&d_{i,n+1}\left(t^*\right)=A_i\left(d_{i,0}\left(t^*\right)+d_{i,1}\left(t^*\right)+...+d_{i,n}\left(t^*\right)\right).
\end{aligned} \tag{58}$$

Consequently, one can obtain the exact solution using the following formula:

$$q_i\left(t^*\right)=\lim_{n\to\infty} q_{i,n}\left(t^*\right)=\sum_{n=0}^{\infty}d_{i,n}\left(t^*\right) \tag{59}$$

Eq. (59) converges to the exact solution, when:

$$0\ll\alpha_{i,j}<1\ ,\quad \left(i=1,2,...,m\right),\left(j=0,1,2,...\right) \tag{60}$$

where,

$$\alpha_{i,j}=\begin{cases}\dfrac{\left\|d_{i,j+1}\left(t^*\right)\right\|}{\left\|d_{i,j(t^*)}\right\|} & \left\|d_{i,j}\left(t^*\right)\right\|\neq 0\\ 0 & \left\|d_{i,j}\left(t^*\right)\right\|\neq 0\end{cases} \tag{61}$$

Verification

To verify the versatility of the presented solution method and its accuracy, using the proposed method, the solution of large amplitude free vibrations of size-dependent circular graphene sheets with various boundary conditions are obtained. The corresponding results are compared with those obtained in Ref[68]. To extract these results, the following material properties were used: E = 1.06 *Tpa*, v = 0.3, ρ = 2300 Kg/m^3, h = 0.34 *nm*, and R=10*nm*.Since the linear problem of free axisymmetric flexural vibration of a circular plate, with simply supported and clamped edge boundary condition, has an exact analytical solution, the selected basic functions $\varphi_i(r)$were taken as the linear free oscillation mode shapes of the circular plates with the boundary conditions given in [97] such that:

$$\varphi_i(r) = I_0(\lambda_i r) - \frac{I_0(\lambda_i)}{J_0(\lambda_i)} J_0(\lambda_i r) \tag{61}$$

In this equation, J_0 and I_0 are the Bessel and the modified Bessel functions of the first kind with zero order, respectively. The positive real values of λ_i for the simply supported and clamped edge boundary conditions are given in Table1. Also, the distribution of normalized functions $\varphi_i(r^*)$ for these two boundary conditions are shown in Fig.2.

Table 1. The positive real value of λ_i for simply supported and clamped edge boundary conditions.

Boundary condition	λ_1	λ_2	λ_3
Simply supported	2.2215	5.4516	8.6114
clamped	3.1962	6.3064	9.4395

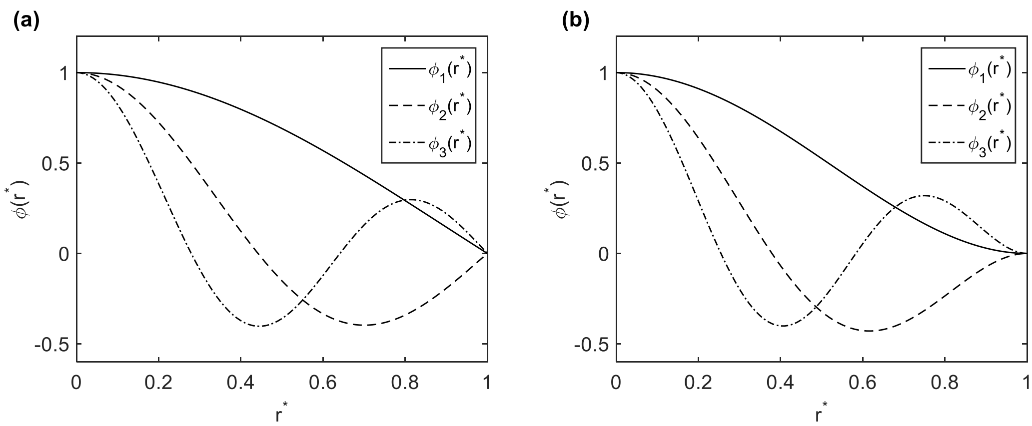

Figure 2. Distribution of functions $\varphi_i(r^*)$ versus r^* based on; (a) simply supported, and (b) clamped boundary conditions.

Additionally, the first two dimensionless frequencies with two different boundary conditions are presented in Table 2, for various nonlocal parameterse_0a. Similar results from Ref.[68]are also presented in this Table, for the purpose of comparison. Excellent agreements are observed between the results of both methods. In addition, from the results in Table 2, it is observed that for a given value of $\Omega_{L,i} = R^2\sqrt{\rho h / D}$, the dimensionless frequencies are increasing monotonically with respect to a decrease in nonlocal parameter e_0a. This behavior is observed for both types of boundary conditions. This comparative study shows that the present approach can yield reliable results for the nonlinear vibration of a nano-plate which is formulated based on the Eringen's model. To further verify the accuracy of the VIM, the relationship between the initial condition ($w^*(0,0)$ =w (0,0) R/h^2) and the ratio of the first dimensionless nonlinear frequency is presented in Tables 3-5, for the first three dimensionless linear frequencies ($\Omega_{Nl,i}/\Omega_{L,i}$, i=1,2,3). These values are based on the various dimensionless nonlocal parameter μ, for the two types of boundary conditions used in this analysis (namely, simply supported and clamped edge constraints). For further comparison, the obtained results are compared with those from Ref. [70]. This reference studies the large amplitude nonlinear free vibrations of a size-dependent nano-disk based on the nonlocal elasticity theory. In this reference, the governing equations were solved using the homotopy perturbation method. As shown, excellent agreements are observed between the results of both methods, for both types of boundary conditions.

Table 2. Comparison of dimensionless frequency for two different boundary conditions and nonlocal parameter ($\Omega_{L,1} = R^2\sqrt{\rho h / D}\ .\ \omega_{L,1}$, $R = 10nm$).

Boundary conditions	$e_0a(nm)$	$\Omega_{L,1}$ Ref [68]	$\Omega_{L,1}$ Present work	$\Omega_{L,2}$ Ref [68]	$\Omega_{L,2}$ Present work
Simply supported	0	4.9345	4.9350	29.7198	29.7199
	0.5	4.8997	4.8996	28.6485	28.6487
	1	4.7979	4.7979	26.0189	26.0188
	1.5	4.6409	4.6415	22.8917	22.8911
	2	4.4455	4.4462	19.9529	19.9515
Clamped	0	10.2158	10.2157	39.7706	39.7707
	0.5	10.1283	10.1284	38.2059	38.2060
	1	9.8784	9.8788	34.4275	34.4289
	1.5	9.4999	9.5001z	30.0446	30.0445
	2	9.0348	9.0357	26.0253	26.0318

Table 3. Comparison of the effect of initial conditions $w^*(0, 0)$ and the ratio of h/R on the first frequency ratio $\Omega_{Nl,1}/\Omega_{L,1}$ of the nano-disk based on the dimensionless nonlocal parameter μ=0.2.

Boundary condition	$w^*(0,0)$	$\Omega_{L,1}$	$\Omega_{Nl,1}/\Omega_{L,1}$ h/R=0.05 Ref.[70]	h/R=0.05 Present work	h/R=0.10 Ref.[70]	h/R=0.10 Present work
Simply supported	0.2	4.4462	1.0001	1.0001	1.0003	1.0004
	0.4		1.0003	1.0003	1.0013	1.0015
	0.6		1.0007	1.0008	1.0029	1.0028
	0.8		1.0013	1.0015	1.0052	1.0053
	1.0		1.0020	1.0019	1.0081	1.0083
Clamped	0.02	9.0398	1.0001	1.0002	1.0006	1.0007
	0.03		1.0006	1.0008	1.0022	1.0023
	0.04		1.0013	1.0014	1.0050	1.0052
	0.05		1.0022	1.0025	1.0089	1.0091
	0.10		1.0035	1.0034	1.0139	1.0139

Table 4. Comparison of the effect of initial conditions $w^*(0, 0)$ and the ratio of h/R on the first frequency ratio $\Omega_{Nl,1}/\Omega_{L,1}$ of the nano-disk based on the dimensionless nonlocal parameter μ=0.2.

Boundary condition	$w^*(0,0)$	$\Omega_{L,2}$	$\Omega_{Nl,2}/\Omega_{L,2}$ h/R=0.05 Ref.[70]	h/R=0.05 Present work	h/R=0.10 Ref.[70]	h/R=0.10 Present work
Simply supported	0.2	19.9515	1.0007	1.0001	1.0003	1.0004
	0.4		1.0029	1.0003	1.0013	1.0015
	0.6		1.0065	1.0008	1.0029	1.0028

	0.8		1.0114	1.0015	1.0052	1.0053
	1.0		1.0178	1.0019	1.0081	1.0083
Clamped	0.02	26.0139	1.0007	1.0002	1.0006	1.0007
	0.03		1.0028	1.0008	1.0022	1.0023
	0.04		1.0062	1.0014	1.0050	1.0052
	0.05		1.0110	1.0025	1.0089	1.0091
	0.10		1.0172	1.0034	1.0139	1.0139

Table 5. Comparison of the effect of initial conditions $w^*(0, 0)$ and the ratio of h/R on the first frequency ratio $\Omega_{Nl,3}/\Omega_{L,3}$ of the nano-disk based on the dimensionless nonlocal parameter μ=0.2.

Boundary condition	$w^*(0,0)$	$\Omega_{L,3}$	$\Omega_{Nl,3}/\Omega_{L,3}$			
			h/R=0.05		h/R=0.10	
			Ref.[70]	Present work	Ref.[70]	Present work
Simply supported	0.2	37.0988	1.0007	1.0006	1.0027	1.0025
	0.4		1.0027	1.0029	1.0106	1.0107
	0.6		1.0060	1.0062	1.0236	1.0235
	0.8		1.0106	1.0106	1.0416	1.0414
	1.0		1.0165	1.0166	1.0643	1.0645
Clamped	0.02	43.5515	1.0012	1.0013	1.0046	1.0045
	0.03		1.0046	1.0046	1.0183	1.0184
	0.04		1.0103	1.0104	1.0407	1.0408
	0.05		1.0183	1.0185	1.0712	1.0713
	0.10		1.0284	1.0283	1.1093	1.1094

In the sequel, the dimensionless central deflection $w^*(0, t^*)$ of the nano-disk with simply supported and clamped edge boundary conditions are obtained versus t^*, using the VIM, as well as the Runge-Kutta 4th order method, for further comparison. To plot the extracted results in Figs. 3 and 4, the following properties along with the initial condition of $w^*(0, 0)$ =1were used; μ=0.1, h/R=0.01 (Fig. 3) and h/R =0.1 (Fig. 4). Excellent agreements were observed between the results of both methods.

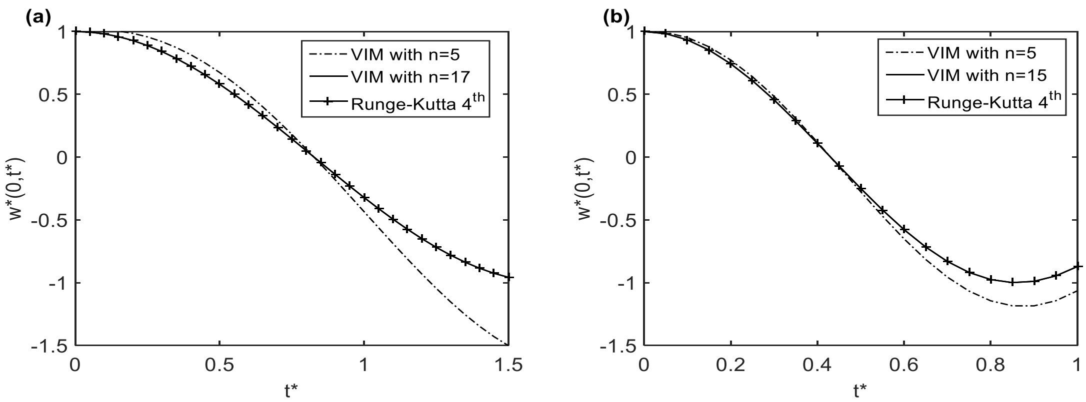

Figure 3. Distribution of dimensionless transverse displacement $w^*(0, t^*)$ of the nano-disk versus t^* for h/R=0.01, based on the VIM and Rung-Kutta 4th order method**,** (**a**) simply supported and (**b**) clamped edge.

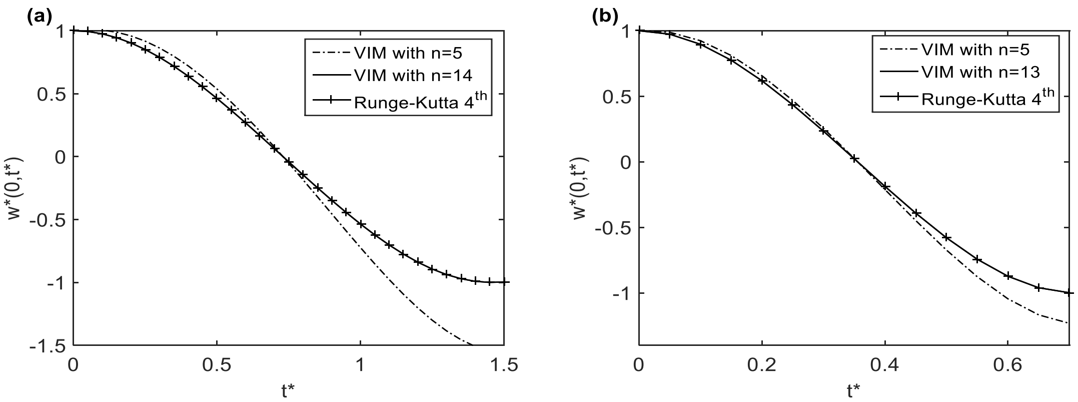

Figure 4. Distribution of dimensionless transverse displacement $w^*(0, t)$ of the nano-disk versus t^*, for h/R=0.1, based on the VIM and Rung-Kutta 4^{th} order method**,** **(**a) simply supported and **(**b) clamped edge.

Numerical results

To further study the influences of the dimensionless non-local parameter μ, initial condition $w^*(0, 0)$, h/R ratio and the associated boundary conditions on the frequency ratio Ω_{Nl}/Ω_L, numerical simulations were used to extract the results, based on a Poisson's ratio of $\upsilon = 0.3$.

For this purpose, for the selected values of $w^*(0,0)$ and h/R ratio shown in Tables 6-8, different values of frequency ratios $\Omega_{Nl,i}/\Omega_{L,\mathrm{I}}$ were selected (values of which are shown in these Tables) for the first three vibration modes (i=1,2,3) of the nano-disk. Here, a value of 0.5 was selected for the non-local parameter μ. Results indicate that for the given values of h/R, the frequency ratio increases with an increase in the initial condition $w^*(0, 0)$. This result is consistent with the sole geometric nonlinearity assumption considered here, according to which the nano-disk exhibits the well-known inherent stiffening vibrational behavior associated with the von Kármán nonlinearity model. On the other hand, it is observed that as the ratio of h/R increases, the frequency ratio increases. The rate of increase in this frequency ratio is faster for the clamped boundary condition, in comparison with the simply supported constraint.

Table 6. The effect of h/R ratio on the first nonlinear frequency ratios, $\Omega_{NL,1}/\Omega_{L,1}$, of the nano-disk in the first mode, μ=0.5 and υ = 0.3.

Boundary condition	h/R	$\Omega_{L,1}$	$w^*(0,0)$				
			0.1	0.2	0.5	0.7	1.0
Simply supported	0.02	3.1529	1.0000	1.0000	1.0001	1.0003	1.0005
	0.05		1.0000	1.0003	1.0008	1.0016	1.0033
	0.08		1.0001	1.0008	1.0021	1.0042	1.0085
	0.10		1.0001	1.0012	1.0033	1.0065	1.0132
Clamped	0.02	6.1806	1.0000	1.0001	1.0004	1.0008	1.0016
	0.05		1.0001	1.0009	1.0025	1.0050	1.0102
	0.08		1.0003	1.0023	1.0065	1.0127	1.0258
	0.10		1.0004	1.0037	1.0102	1.0198	1.0400

Table 7. The effect of *h/R* on the second nonlinear frequency ratios, $\Omega_{NL,2}/\Omega_{L,2}$, of the nano-disk in the second mode, μ= 0.5 and υ = 0.3.

Boundary condition	*h/R*	$\Omega_{L,1}$	$w^*(0,0)$				
			0.1	0.2	0.5	0.7	1.0
Simply supported	0.02	10.1236	1.0000	1.0002	1.0005	1.0010	1.0021
	0.05		1.0001	1.0012	1.0033	1.0065	1.0132
	0.08		1.0003	1.0031	1.0085	1.0165	1.0334
	0.10		1.0005	1.0048	1.0132	1.0257	1.0518
Clamped	0.02	13.0006	1.0001	1.0007	1.0021	1.0041	1.0083
	0.05		1.0005	1.0047	1.0129	1.0252	1.0508
	0.08		1.0013	1.0119	1.0328	1.0633	1.1254
	0.10		1.0021	1.0186	1.0508	1.0973	1.1901

Table 8. The effect of *h/R* on the third nonlinear frequency ratios, $\Omega_{NL,3}/\Omega_{L,3}$, of the nano-disk in the third mode, μ= 0.5 and υ = 0.3.

Boundary condition	*h/R*	$\Omega_{L,1}$	$w^*(0,0)$				
			0.1	0.2	0.5	0.7	1.0
Simply supported	0.02	16.6983	1.0001	1.0005	1.0013	1.0024	1.0050
	0.05		1.0003	1.0028	1.0078	1.0152	1.0308
	0.08		1.0008	1.0072	1.0198	1.0385	1.0771
	0.10		1.0013	1.0112	1.0308	1.0595	1.1181
Clamped	0.02	19.4850	1.0002	1.0018	1.0051	1.0100	1.0202
	0.05		1.0013	1.0114	1.0315	1.0608	1.1205
	0.08		1.0033	1.0290	1.0787	1.1492	1.2862
	0.10		1.0051	1.0450	1.1205	1.2251	1.4221

The influence of dimensionless non-local parameter μ on the frequency ratio Ω_{NL}/Ω_L are shown in Figs. 5 and 6, for a simply supported nano-disk based on different values of μ and the two values of h/R=0.01(Fig. 5) and h/R=0.1(Fig. 6). Similar plots are shown in Figs.7 and 8 for the nano-disk based on a clamped boundary condition. The frequency ratios $\Omega_{Nl,i}/\Omega_{Li}$ for the first three modes (i=1,2,3) that are calculated and plotted in Fig.5-8, are based on the Poisson's ratio of 0.3.Inthese figures, the frequency ratios increase monotonically with an increase in dimensionless non-local parameter μ.The rate of increase is higher at higher values of initial condition $w^*(0,0)$,as well as for the clamped edge boundary condition .Comparison of different cases in each figure reveals that the effect of non-local parameter μon the frequency ratio is less prominent at lower modes of vibration.

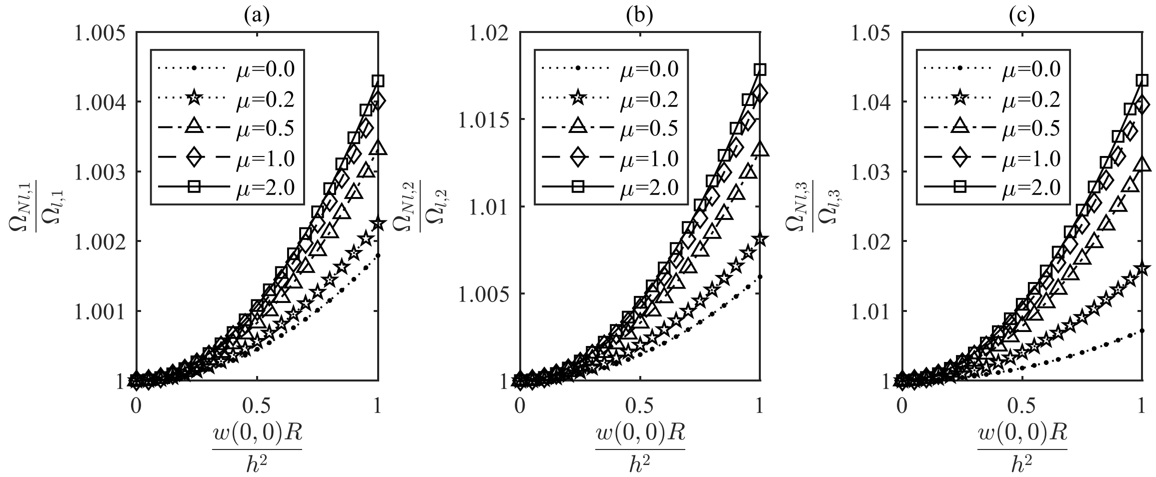

Figure 5. The effects of dimensionless nonlocal parameterμ and initial conditions, $w^*(0,0)$ $=w$ $(0,0)$ R/h^2, on the frequency ratios (Ω_{NL}/Ω_L) of the **simply supported nano-disk** with ***h/R*=0.05**. **(**a**)** first mode, **(**b**)** second mode, and **(**c**)** third mode.

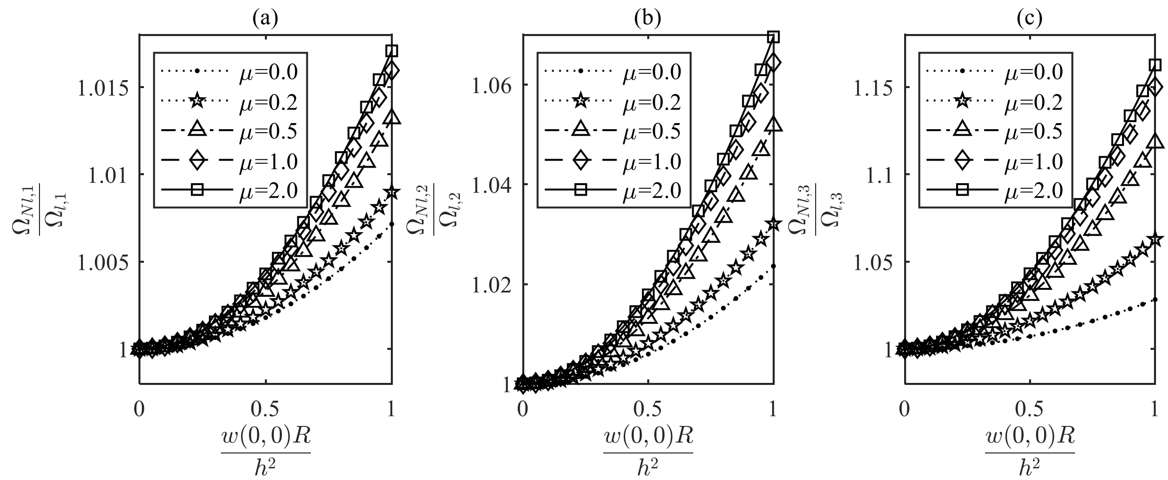

Figure 6. The effects of dimensionless nonlocal parameter μ and initial conditions, $w^*(0, 0)$ $=w(0,0)$ R/h^2, on the frequency ratios (Ω_{NL}/Ω_L)of the **simply supported nano-disk** with ***h/R*=0.1**. **(**a**)** first mode, **(**b**)** second mode, and **(**c**)** third mode.

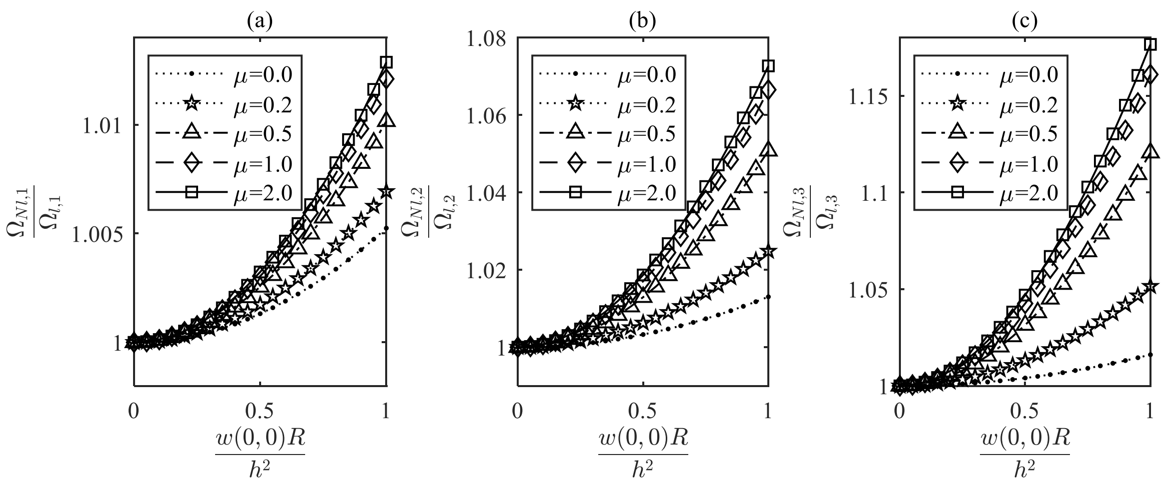

Figure 7. The effects of dimensionless nonlocal parameter μ and initial conditions, $w^*(0,0)$ $=w$ $(0,0)$ R/h^2, on the frequency ratios (Ω_{NL}/Ω_L) of the **clamped nano-disk** with ***h/R*=0.05**. **(**a**)** first mode, **(**b**)** second mode, and **(**c**)** third mode.

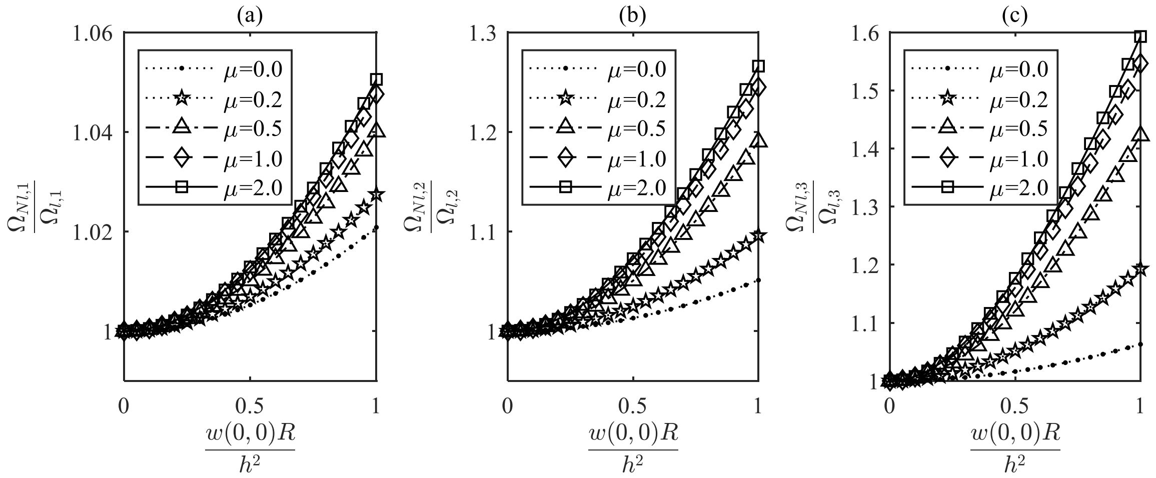

Figure 8. The effects of dimensionless nonlocal parameter μ and initial conditions, $w^{*}(0,0)$ $=w$ $(0,0)$ R/h^{2}, on the frequency ratios (Ω_{NL}/Ω_{L}) of the **clamped nano-disk** with ***h/R*=0.1**. **(a)** first mode, **(b)** second mode, and **(c)** third mode.

Figures 9-12 illustrate dependency of frequency ratio (Ω_{NL}/Ω_{L}) on *h/R*, for different values of μ and the two initial conditions of $w^{*}(0,0)$ =0.5 and $w^{*}(0,0)$ =1.0. The selected boundary conditions are assumed to simply supported and clamped. It is observed that based on the nonlocal elasticity theory, the *h/R* ratio plays an important role in the nonlinear frequencies, while according to the local theory (μ=0) its effect is minute. Moreover, according to the nonlocal elasticity theory, the effect of *h/R* is more pronounced at higher values of nonlocal parameter μ, higher modes of vibration, as well as the clamped edge boundary condition.

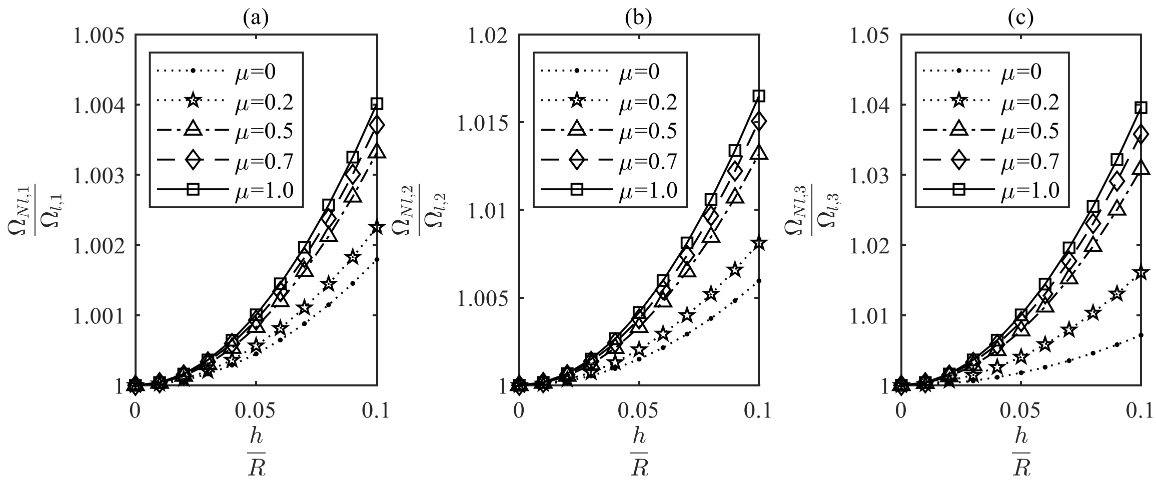

Figure 9. The effects of (*h/R*) ratio and dimensionless nonlocal parameter μ on the frequency ratio (Ω_{NL}/Ω_{L}) for a **simply supported nano-disk** with $\mathbf{w^{*}(0,0)}$ **=0.5**. (a) first mode, (b) second mode, and (c)third mode of vibration.

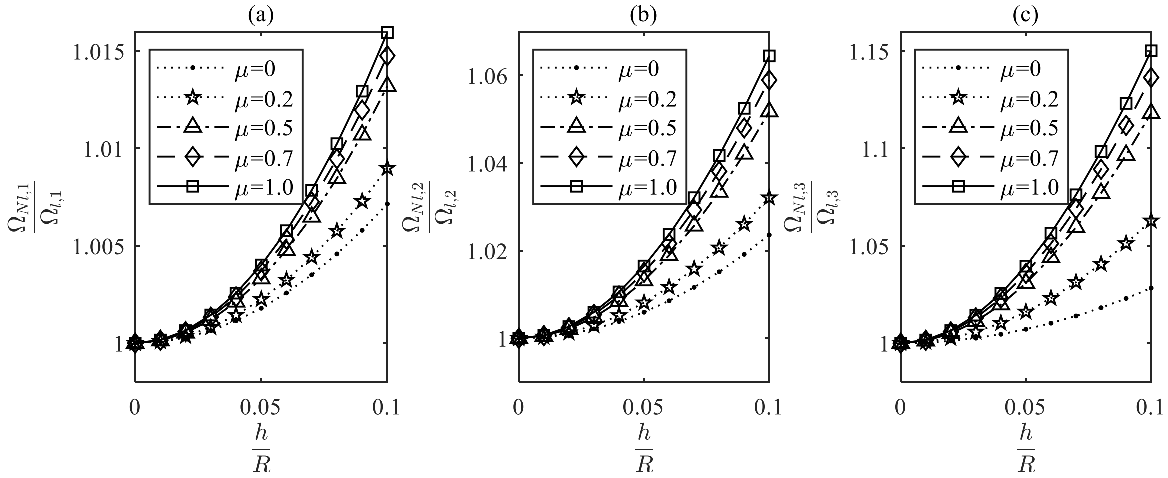

Figure 10. The effects of (*h/R*) ratio and dimensionless nonlocal parameterμ on the frequency ratio (Ω_{NL}/Ω_L) for a **simply supported nano-disk** with $\boldsymbol{w^*(0,0)=1.0}$. (a) first mode, (b) second mode, and (c) third mode of vibration.

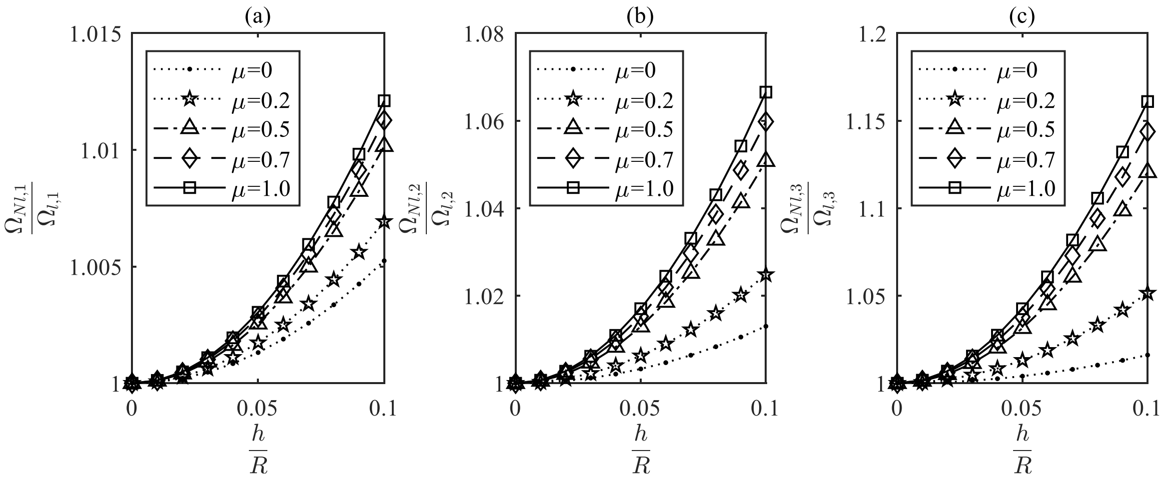

Figure 11. The effects of (*h/R*) ratio and dimensionless nonlocal parameterμ on the frequency ratio (Ω_{NL}/Ω_L) for **a clamped nano-disk** with $\boldsymbol{w^*(0,0)=0.5}$. (a) first mode, (b) second mode, and (c) third mode of vibration.

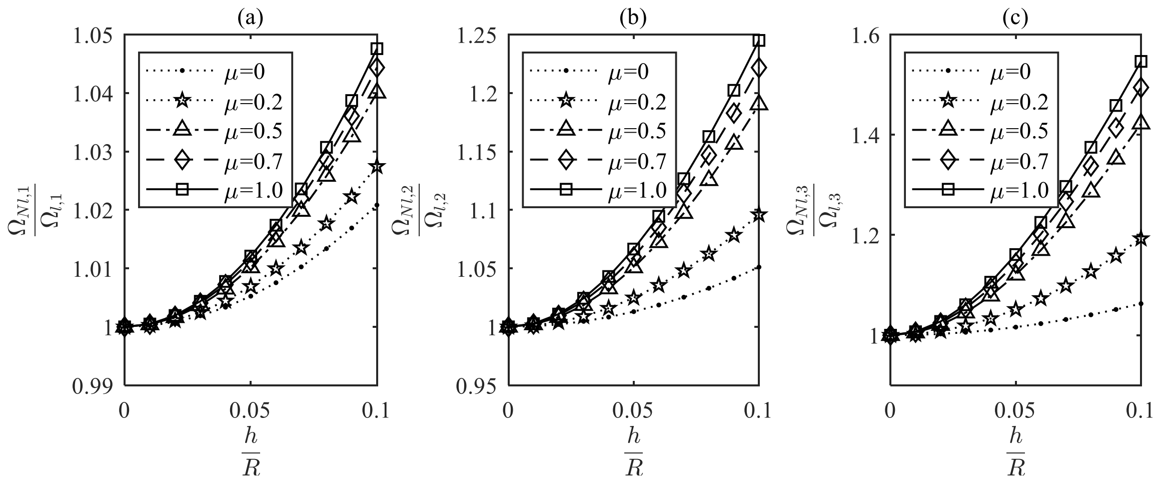

Figure 12. The effects of (*h/R*) ratio and dimensionless nonlocal parameterμ on the frequency ratio (Ω_{NL}/Ω_L) for a **clamped nano-disk** with $\boldsymbol{w^*(0,0)=1.0}$. (a) first mode, (b) second mode, and (c) third mode of vibration.

The vibrational transverse displacements of the clamped and simply supported nano-disk with $w(0,0)\ R/h^2 = 1.0$are displayed in Figs.13 and 14.The used value of h/R is equal to 1.0.To perform the corresponding calculations, the geometric and mechanical properties used to generate the data in Table 2 were used. For the purpose of comparison, the corresponding results from the local theory of plate are also superimposed.

The differences in transverse displacements predicted by the local and nonlocal models can be clearly observed in both figures. This difference is less prominent for smaller nonlocal parameterμ. Consequently, one can conclude that the nonlocal parameter has a major effect on the vibrational transverse displacement and modeling a nano-disk based on the classical theory creates erroneous results.

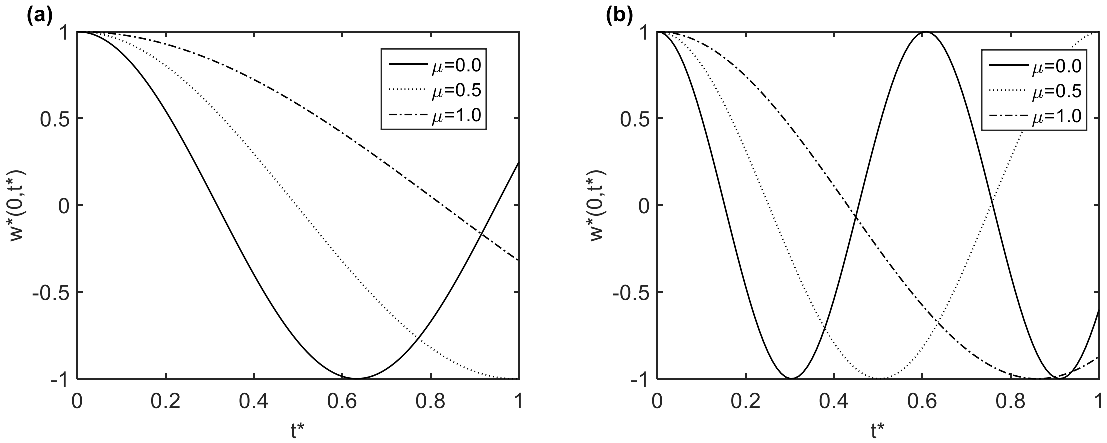

Figure 13. The effect of dimensionless nonlocal parameter μon the dimensionless transverse displacement $w^*(0, t^*)$ of the nano-disk, based on h/R=0.01and $w^*(0, 0)$ =1.0 for, **(**a) simply supported condition, and **(**b) clamped edge condition.

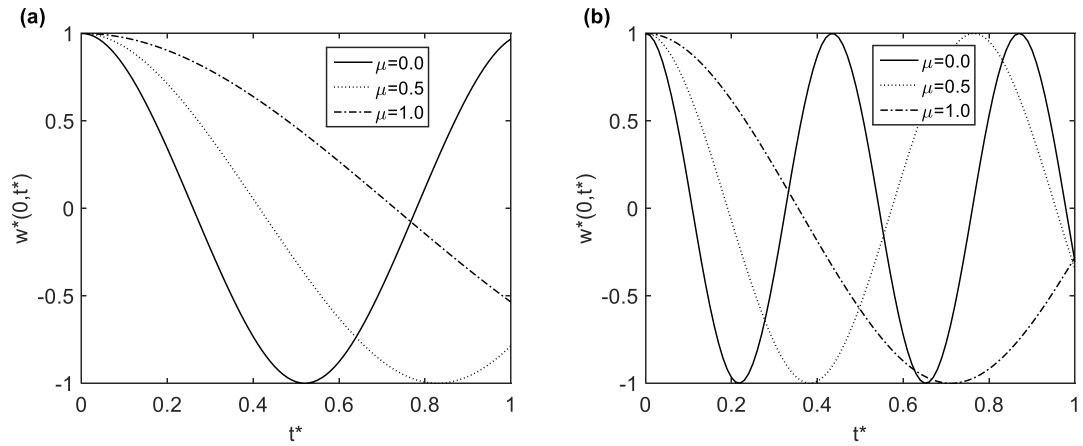

Figure 14. The effect of dimensionless nonlocal parameter μ on the dimensionless transverse displacement $w^*(0, t^*)$ of the nano-disk, based on h/R=0.1 and $w^*(0, 0)$ =1.0for, **(**a) simply supported condition, and **(**b) clamped edge condition.

Conclusion

A new method for the solution of nonlinear free vibration of a nano-disk (nano circular plate) was formulated by applying Hamilton's principle, based on the nonlocal elasticity and von Kármán geometrically nonlinear theories. The proposed model was size-dependent with an additional material length scale parameter to capture the size effect. The deduced governing equations were formulated such that they could be reduced to those of local elasticity theory provided $\mu=0$. The Galerkin weighted residual method, in conjunction with the VIM, was used to solve the governing equations for the two simply supported and clamped edge boundary conditions. The applied method proved to be straightforward, useful, and a powerful technique for providing a solution for nonlinear characteristic relation of the dimensionless frequency versus amplitude, as well as the mode shape functions, when size effect is included. Results indicated that for all values of the nonlocal parameter μ, the linear natural frequencies predicted by the local theory are greater than those predicted by the nonlocal elasticity theory. This result was consistent with the sole geometric nonlinearity assumption according to which the nano-disk exhibits the well-known inherent stiffening behavior associated with the von Kármán nonlinearity model. Moreover, increasing the value of dimensionless nonlocal parameter, increased the effect of central dimensionless amplitude on the nonlinear frequencies. This effect was more at higher vibrational modes. Additionally, it was observed that the ratio of *h/R* plays an important role in the nonlinear frequencies, while according to the local theory of elasticity, its effect appears to be minute. However, results indicated that the nonlocal effect may be ignored when the thickness to radius ratio, *h/R*, is very small. Further examination of the results on both boundary conditions indicated that there is a considerable difference between the predicted values of frequencies and transverse displacements, obtained from the local and nonlocal models.

References

[1] P. Ball, Roll up for the revolution, Nature Publishing Group, 2001.

[2] R. H. Baughman, A. A. Zakhidov, W. A. De Heer, Carbon nanotubes--the route toward applications, *science,* Vol. 297, No. 5582, pp. 787-792, 2002.

[3] B. Bodily, C. Sun, Structural and equivalent continuum properties of single-walled carbon nanotubes, *International Journal of Materials and Product Technology,* Vol. 18, No. 4-6, pp. 381-397, 2003.

[4] C. Li, T.-W. Chou, A structural mechanics approach for the analysis of carbon nanotubes, *International Journal of Solids and Structures,* Vol. 40, No. 10, pp. 2487-2499, 2003.

[5] C. Li, T.-W. Chou, Single-walled carbon nanotubes as ultrahigh frequency nanomechanical resonators, *Physical review B,* Vol. 68, No. 7, pp. 073405, 2003.

[6] S. Pradhan, J. Phadikar, Nonlinear analysis of carbon nanotubes, Proceedings of Fifth International Conference on Smart Materials, *Structures and Systems, Indian Institute of Science, Bangalore,* pp. 24-26, 2008.

[7] A. Chong, F. Yang, D. C. Lam, P. Tong, Torsion and bending of micron-scaled structures, *Journal of Materials Research,* Vol. 16, No. 4, pp. 1052-1058, 2001.

[8] N. Fleck, G. Muller, M. Ashby, J. Hutchinson, Strain gradient plasticity: theory and experiment, *Acta Metallurgica et Materialia,* Vol. 42, No. 2, pp. 475-487, 1994.

[9] Z. E. Hajilak, J. Pourghader, D. Hashemabadi, F. S. Bagh, M. Habibi, H. Safarpour, Multilayer GPLRC composite cylindrical nanoshell using modified strain gradient theory, *Mechanics Based Design of Structures and Machines*, 2019.

[10] C. Lim, G. Zhang, J. Reddy, A higher-order nonlocal elasticity and strain gradient theory and its applications in wave propagation, *Journal of the Mechanics and Physics of Solids,* Vol. 78, pp. 298-313, 2015.

[11] A. Babaei, A. Rahmani, Vibration analysis of rotating thermally-stressed gyroscope, based on modified coupled displacement field method, *Mechanics based design of structures and machines*, pp. 1-10, 2020.

[12] M. Mohammadimehr, M. Mahmudian-Najafabadi, Bending and free vibration analysis of nonlocal functionally graded nanocomposite timoshenko beam model rreinforced by swbnnt based on modified coupled stress theory, *Journal of Nanostructures,* Vol. 3, No. 4, pp. 483-492, 2013.

[13] C. H. Thai, A. Ferreira, H. Nguyen-Xuan, P. Phung-Van, A size dependent meshfree model for functionally graded plates based on the nonlocal strain gradient theory, *Composite Structures,* Vol. 272, pp. 114169, 2021.

[14] G. T. Monaco, N. Fantuzzi, F. Fabbrocino, R. Luciano, Hygro-thermal vibrations and buckling of laminated nanoplates via nonlocal strain gradient theory, *Composite Structures,* Vol. 262, pp. 113337, 2021.

[15] M. Ebrahimian, A. Imam, M. Najafi, Doublet mechanical analysis of bending of Euler-Bernoulli and Timoshenko nanobeams, *ZAMM-Journal of Applied Mathematics and Mechanics/Zeitschrift für Angewandte Mathematik und Mechanik,* Vol. 98, No. 9, pp. 1642-1665, 2018.

[16] M. Ebrahimian, A. Imam, M. Najafi, The effect of chirality on the torsion of nanotubes embedded in an elastic medium using doublet mechanics, *Indian Journal of Physics,* Vol. 94, No. 1, pp. 31-45, 2020.

[17] M. Emadi, M. Z. Nejad, S. Ziaee, A. Hadi, Buckling analysis of arbitrary two-directional functionally graded nano-plate based on nonlocal elasticity theory using generalized differential quadrature method, *Steel and Composite Structures,* Vol. 39, No. 5, pp. 565-581, 2021.

[18] E. Zarezadeh, V. Hosseini, A. Hadi, Torsional vibration of functionally graded nano-rod under magnetic field supported by a generalized torsional foundation based on nonlocal elasticity theory, *Mechanics Based Design of Structures and Machines,* Vol. 48, No. 4, pp. 480-495, 2020.

[19] L. Shen, H.-S. Shen, C.-L. Zhang, Nonlocal plate model for nonlinear vibration of single layer graphene sheets in thermal environments, *Computational Materials Science,* Vol. 48, No. 3, pp. 680-685, 2010.

[20] S. Ramezani, A micro scale geometrically non-linear Timoshenko beam model based on strain gradient elasticity theory, *International Journal of Non-Linear Mechanics,* Vol. 47, No. 8, pp. 863-873, 2012.

[21] E. Jomehzadeh, A. Saidi, Study of small scale effect on nonlinear vibration of nano-plates, *Journal of Computational and Theoretical Nanoscience,* Vol. 9, No. 6, pp. 864-871, 2012.

[22] X. He, J. Wang, B. Liu, K. M. Liew, Analysis of nonlinear forced vibration of multi-layered graphene sheets, *Computational Materials Science,* Vol. 61, pp. 194-199, 2012.

[23] S. Ramezani, Nonlinear vibration analysis of micro-plates based on strain gradient elasticity theory, *Nonlinear Dynamics,* Vol. 73, No. 3, pp. 1399-1421, 2013.

[24] L. Zhang, Y. Zhang, K. Liew, Modeling of nonlinear vibration of graphene sheets using a meshfree method based on nonlocal elasticity theory, *Applied Mathematical Modelling,* Vol. 49, pp. 691-704, 2017.

[25] M. Mohammadi, M. Hosseini, M. Shishesaz, A. Hadi, A. Rastgoo, Primary and secondary resonance analysis of porous functionally graded nanobeam resting on a nonlinear foundation subjected to mechanical and electrical loads, *European Journal of Mechanics-A/Solids,* Vol. 77, pp. 103793, 2019.

[26] M. Z. Nejad, A. Hadi, A. Omidvari, A. Rastgoo, Bending analysis of bi-directional functionally graded Euler-Bernoulli nano-beams using integral form of Eringen's non-local elasticity theory, *Structural engineering and mechanics: An international journal,* Vol. 67, No. 4, pp. 417-425, 2018.

[27] M. M. Adeli, A. Hadi, M. Hosseini, H. H. Gorgani, Torsional vibration of nano-cone based on nonlocal strain gradient elasticity theory, *The European Physical Journal Plus,* Vol. 132, No. 9, pp. 393, 2017/09/18, 2017.

[28] M. Shishesaz, M. Hosseini, K. Naderan Tahan, A. Hadi, Analysis of functionally graded nanodisks under thermoelastic loading based on the strain gradient theory, *Acta Mechanica,* Vol. 228, No. 12, pp. 4141-4168, 2017/12/01, 2017.

[29] M. Hosseini, A. Hadi, A. Malekshahi, M. Shishesaz, A review of size-dependent elasticity for nanostructures, *Journal of Computational Applied Mechanics,* Vol. 49, No. 1, pp. 197-211, 2018.

[30] M. Mousavi Khoram, M. Hosseini, M. Shishesaz, A concise review of nano-plates, *Journal of Computational Applied Mechanics,* Vol. 50, No. 2, pp. 420-429, 2019.

[31] A. Daneshmehr, A. Rajabpoor, A. Hadi, Size dependent free vibration analysis of nanoplates made of functionally graded materials based on nonlocal elasticity theory with high order theories, *International Journal of Engineering Science,* Vol. 95, pp. 23-35, 2015.

[32] H. Haghshenas Gorgani, M. Mahdavi Adeli, M. Hosseini, Pull-in behavior of functionally graded micro/nano-beams for MEMS and NEMS switches, *Microsystem Technologies,* Vol. 25, No. 8, pp. 3165-3173, 2019/08/01, 2019.

[33] A. Hadi, M. Z. Nejad, A. Rastgoo, M. Hosseini, Buckling analysis of FGM Euler-Bernoulli nano-beams with 3D-varying properties based on consistent couple-stress theory, *Steel and Composite Structures,* Vol. 26, No. 6, pp. 663-672, 2018.

[34] A. Barati, M. M. Adeli, A. Hadi, Static torsion of bi-directional functionally graded microtube based on the couple stress theory under magnetic field, *International Journal of Applied Mechanics,* Vol. 12, No. 02, pp. 2050021, 2020.

[35] A. Barati, A. Hadi, M. Z. Nejad, R. Noroozi, On vibration of bi-directional functionally graded nanobeams under magnetic field, *Mechanics Based Design of Structures and Machines*, pp. 1-18, 2020.

[36] K. Dehshahri, M. Z. Nejad, S. Ziaee, A. Niknejad, A. Hadi, Free vibrations analysis of arbitrary three-dimensionally FGM nanoplates, *Advances in nano research,* Vol. 8, No. 2, pp. 115-134, 2020.

[37] M. Moraveji, H. Keshvari, A. Karkhaneh, S. Bonakdar, A. Hadi, N. Haghighipour, The effect of collagen/polycaprolactone fibrous scaffold decorated with graphene nanoplatelet and low-frequency

electromagnetic field on neuronal gene expression by stem cells, *Advances in nano research*, Vol. 10, No. 6, pp. 549-557, 2021.
[38] M. Najafzadeh, M. M. Adeli, E. Zarezadeh, A. Hadi, Torsional vibration of the porous nanotube with an arbitrary cross-section based on couple stress theory under magnetic field, *Mechanics Based Design of Structures and Machines*, pp. 1-15, 2020.
[39] H. Nekounam, R. Dinarvand, R. Khademi, F. Asghari, N. Mahmoodi, H. Arzani, E. Hasanzadeh, A. Hadi, R. Karimi, M. Kamali, Preparation of cationized albumin nanoparticles loaded indirubin by high pressure hemogenizer, *bioRxiv*, 2021.
[40] A. Soleimani, K. Dastani, A. Hadi, M. H. Naei, Effect of out-of-plane defects on the postbuckling behavior of graphene sheets based on nonlocal elasticity theory, *Steel and Composite Structures*, Vol. 30, No. 6, pp. 517-534, 2019.
[41] M. Shishesaz, M. Hosseini, K. N. Tahan, A. Hadi, Analysis of functionally graded nanodisks under thermoelastic loading based on the strain gradient theory, *Acta Mechanica*, Vol. 228, No. 12, pp. 4141-4168, 2017.
[42] M. M. Khoram, M. Hosseini, A. Hadi, M. Shishehsaz, Bending Analysis of Bidirectional FGM Timoshenko Nanobeam Subjected to Mechanical and Magnetic Forces and Resting on Winkler–Pasternak Foundation, *International Journal of Applied Mechanics*, Vol. 12, No. 08, pp. 2050093, 2020.
[43] A. Hadi, A. Rastgoo, N. Haghighipour, A. Bolhassani, Numerical modelling of a spheroid living cell membrane under hydrostatic pressure, *Journal of Statistical Mechanics: Theory and Experiment*, Vol. 2018, No. 8, pp. 083501, 2018.
[44] R. Noroozi, A. Barati, A. Kazemi, S. Norouzi, A. Hadi, Torsional vibration analysis of bi-directional FG nano-cone with arbitrary cross-section based on nonlocal strain gradient elasticity, *Advances in nano research*, Vol. 8, No. 1, pp. 13-24, 2020.
[45] A. Hadi, M. Z. Nejad, M. Hosseini, Vibrations of three-dimensionally graded nanobeams, *International Journal of Engineering Science*, Vol. 128, pp. 12-23, 2018.
[46] N.-C. Tsai, J.-S. Liou, C.-C. Lin, T. Li, Analysis and fabrication of reciprocal motors applied for microgyroscopes, *Journal of Micro/Nanolithography, MEMS, and MOEMS*, Vol. 8, No. 4, pp. 043046, 2009.
[47] N.-C. Tsai, J.-S. Liou, C.-C. Lin, T. Li, Design of micro-electromagnetic drive on reciprocally rotating disc used for micro-gyroscopes, *Sensors and Actuators A: Physical*, Vol. 157, No. 1, pp. 68-76, 2010.
[48] N.-C. Tsai, J.-S. Liou, C.-C. Lin, T. Li, Suppression of dynamic offset of electromagnetic drive module for micro-gyroscope, *Mechanical Systems and Signal Processing*, Vol. 25, No. 2, pp. 680-693, 2011.
[49] S. Lee, D. Kim, M. D. Bryant, F. F. Ling, A micro corona motor, *Sensors and Actuators A: Physical*, Vol. 118, No. 2, pp. 226-232, 2005.
[50] K. J. Vahala, Optical microcavities, *nature*, Vol. 424, No. 6950, pp. 839, 2003.
[51] R. W. Boyd, J. E. Heebner, Sensitive disk resonator photonic biosensor, *Applied optics*, Vol. 40, No. 31, pp. 5742-5747, 2001.
[52] A. Dolatabady, N. Granpayeh, V. F. Nezhad, A nanoscale refractive index sensor in two dimensional plasmonic waveguide with nanodisk resonator, *Optics Communications*, Vol. 300, pp. 265-268, 2013.
[53] Y. Zhang, S. Tekobo, Y. Tu, Q. Zhou, X. Jin, S. A. Dergunov, E. Pinkhassik, B. Yan, Permission to enter cell by shape: nanodisk vs nanosphere, *ACS applied materials & interfaces*, Vol. 4, No. 8, pp. 4099-4105, 2012.
[54] I. Hwang, J. Choi, S. Hong, J.-S. Kim, I.-S. Byun, J. H. Bahng, J.-Y. Koo, S.-O. Kang, B. H. Park, Direct investigation on conducting nanofilaments in single-crystalline Ni/NiO core/shell nanodisk arrays, *Applied Physics Letters*, Vol. 96, No. 5, pp. 053112, 2010.
[55] C. Horejs, D. Pum, U. B. Sleytr, H. Peterlik, A. Jungbauer, R. Tscheliessnig, Surface layer protein characterization by small angle x-ray scattering and a fractal mean force concept: from protein structure to nanodisk assemblies, *The Journal of chemical physics*, Vol. 133, No. 17, pp. 11B602, 2010.
[56] C. Hägglund, M. Zäch, G. Petersson, B. Kasemo, Electromagnetic coupling of light into a silicon solar cell by nanodisk plasmons, *Applied physics letters*, Vol. 92, No. 5, pp. 053110, 2008.
[57] C.-H. Huang, M. Igarashi, S. Horita, M. Takeguchi, Y. Uraoka, T. Fuyuki, I. Yamashita, S. Samukawa, Novel Si nanodisk fabricated by biotemplate and defect-free neutral beam etching for solar cell application, *Japanese Journal of Applied Physics*, Vol. 49, No. 4S, pp. 04DL16, 2010.
[58] T. Ito, A. A. Audi, G. P. Dible, Electrochemical characterization of recessed nanodisk-array electrodes prepared from track-etched membranes, *Analytical chemistry*, Vol. 78, No. 19, pp. 7048-7053, 2006.
[59] T. Ito, D.-M. Perera, Electrochemical studies of recessed nanodisk-array electrodes prepared from track-etched membranes, in *Proceeding of*, The Electrochemical Society, pp. 1325-1325.
[60] L. Luo, H. S. White, Electrogeneration of single nanobubbles at sub-50-nm-radius platinum nanodisk electrodes, *Langmuir*, Vol. 29, No. 35, pp. 11169-11175, 2013.

[61] M. K. Chin, D. Y. Chu, S. T. Ho, Estimation of the spontaneous emission factor for microdisk lasers via the approximation of whispering gallery modes, *Journal of applied physics,* Vol. 75, No. 7, pp. 3302-3307, 1994.

[62] H. Cao, J. Xu, W. Xiang, Y. Ma, S.-H. Chang, S.-T. Ho, G. Solomon, Optically pumped InAs quantum dot microdisk lasers, *Applied Physics Letters,* Vol. 76, No. 24, pp. 3519-3521, 2000.

[63] S. J. Choi, K. Djordjev, S. J. Choi, P. D. Dapkus, Microdisk lasers vertically coupled to output waveguides, *IEEE Photonics technology letters,* Vol. 15, No. 10, pp. 1330-1332, 2003.

[64] J. Van Campenhout, P. Rojo-Romeo, P. Regreny, C. Seassal, D. Van Thourhout, S. Verstuyft, L. Di Cioccio, J.-M. Fedeli, C. Lagahe, R. Baets, Electrically pumped InP-based microdisk lasers integrated with a nanophotonic silicon-on-insulator waveguide circuit, *Optics express*, Vol. 15, No. 11, pp. 6744-6749, 2007.

[65] S.-H. Kwon, J.-H. Kang, S.-K. Kim, H.-G. Park, Surface plasmonic nanodisk/nanopan lasers, *IEEE Journal of Quantum Electronics,* Vol. 47, No. 10, pp. 1346-1353, 2011.

[66] S.-Y. Cho, N. M. Jokerst, A polymer microdisk photonic sensor integrated onto silicon, *IEEE photonics technology letters,* Vol. 18, No. 20, pp. 2096-2098, 2006.

[67] Y.-G. Wang, W.-H. Lin, N. Liu, Large amplitude free vibration of size-dependent circular microplates based on the modified couple stress theory, *International Journal of Mechanical Sciences,* Vol. 71, pp. 51-57, 2013.

[68] M. Mohammadi, M. Ghayour, A. Farajpour, Free transverse vibration analysis of circular and annular graphene sheets with various boundary conditions using the nonlocal continuum plate model, *Composites Part B: Engineering,* Vol. 45, No. 1, pp. 32-42, 2013.

[69] M. Hosseini, M. Shishesaz, K. N. Tahan, A. Hadi, Stress analysis of rotating nano-disks of variable thickness made of functionally graded materials, *International Journal of Engineering Science,* Vol. 109, pp. 29-53, 2016.

[70] M. Shishesaz, M. Shariati, A. Yaghootian, A. Alizadeh, Nonlinear Vibration Analysis of Nano-Disks Based on Nonlocal Elasticity Theory Using Homotopy Perturbation Method, *International Journal of Applied Mechanics*, pp. 1950011, 2019.

[71] M. Hosseini, M. Shishesaz, A. Hadi, Thermoelastic analysis of rotating functionally graded micro/nanodisks of variable thickness, *Thin-Walled Structures,* Vol. 134, pp. 508-523, 2019.

[72] M. Shishesaz, M. Shariati, A. Yaghootian, Nonlocal Elasticity Effect on Linear Vibration of Nano-circular Plate Using Adomian Decomposition Method, *Journal of Applied and Computational Mechanics,* Vol. 6, No. 1, pp. 63-76, 2020.

[73] M. Shariati, B. Azizi, M. Hosseini, M. Shishesaz, On the calibration of size parameters related to non-classical continuum theories using molecular dynamics simulations, *International Journal of Engineering Science,* Vol. 168, pp. 103544, 2021.

[74] M. Shishesaz, M. Shariati, M. Hosseini, Size effect analysis on Vibrational response of Functionally Graded annular nano plate based on Nonlocal stress-driven method, *International Journal of Structural Stability and Dynamics*, 2021, In press.

[75] A. C. Eringen, On differential equations of nonlocal elasticity and solutions of screw dislocation and surface waves, *Journal of applied physics,* Vol. 54, No. 9, pp. 4703-4710, 1983.

[76] S. S. Rao, 2019, *Vibration of continuous systems*, Wiley,

[77] M. Amabili, 2008, *Nonlinear vibrations and stability of shells and plates*, Cambridge University Press,

[78] C.-Y. Chia, 1980, *Nonlinear analysis of plates*, McGraw-Hill International Book Company,

[79] S. P. Timoshenko, S. Woinowsky-Krieger, 1959, *Theory of plates and shells*, McGraw-hill,

[80] W. F. Faris, *Nonlinear dynamics of annular and circular plates under thermal and electrical loadings*, Thesis, Virginia Tech, 2003.

[81] C. Wang, J. N. Reddy, K. Lee, 2000, *Shear deformable beams and plates: Relationships with classical solutions*, Elsevier,

[82] J.-H. He, Variational iteration method for autonomous ordinary differential systems, *Applied Mathematics and Computation*, Vol. 114, No. 2-3, pp. 115-123, 2000.

[83] J.-H. He, Some asymptotic methods for strongly nonlinear equations, *International journal of Modern physics B,* Vol. 20, No. 10, pp. 1141-1199, 2006.

[84] J.-H. He, Variational iteration method—some recent results and new interpretations, *Journal of computational and applied mathematics,* Vol. 207, No. 1, pp. 3-17, 2007.

[85] J.-H. He, Variational approach for nonlinear oscillators, *Chaos, Solitons & Fractals,* Vol. 34, No. 5, pp. 1430-1439, 2007.

[86] S. Momani, Z. Odibat, Numerical comparison of methods for solving linear differential equations of fractional order, *Chaos, Solitons & Fractals,* Vol. 31, No. 5, pp. 1248-1255, 2007.

[87] Z. Odibat, S. Momani, Application of variational iteration method to nonlinear differential equations of fractional order, *International Journal of Nonlinear Sciences and Numerical Simulation,* Vol. 7, No. 1, pp. 27-34, 2006.

[88] N. Bildik, A. Konuralp, The use of variational iteration method, differential transform method and Adomian decomposition method for solving different types of nonlinear partial differential equations, *International Journal of Nonlinear Sciences and Numerical Simulation,* Vol. 7, No. 1, pp. 65-70, 2006.

[89] N. Sweilam, M. Khader, Variational iteration method for one dimensional nonlinear thermoelasticity, *Chaos, Solitons & Fractals,* Vol. 32, No. 1, pp. 145-149, 2007.

[90] S. Momani, S. Abuasad, Application of He's variational iteration method to Helmholtz equation, *Chaos, Solitons & Fractals,* Vol. 27, No. 5, pp. 1119-1123, 2006.

[91] A. Soliman, A numerical simulation and explicit solutions of KdV-Burgers' and Lax's seventh-order KdV equations, *Chaos, Solitons & Fractals,* Vol. 29, No. 2, pp. 294-302, 2006.

[92] M. Inokuti, H. Sekine, T. Mura, General use of the Lagrange multiplier in nonlinear mathematical physics, *Variational method in the mechanics of solids,* Vol. 33, No. 5, pp. 156-162, 1978.

[93] J. He, *A new approach to establishing generalized variational principles in fluids and CC Liu constraints*, Thesis, Ph. D. Thesis, Shanghai University, 1996 (in Chinese), 1996.

[94] A.-M. Wazwaz, 2010, *Partial differential equations and solitary waves theory*, Springer Science & Business Media,

[95] S. Abbasbandy, Improving Newton–Raphson method for nonlinear equations by modified Adomian decomposition method, *Applied Mathematics and Computation*, Vol. 145, No. 2-3, pp. 887-893, 2003.

[96] Z. M. Odibat, A study on the convergence of variational iteration method, *Mathematical and Computer Modelling,* Vol. 51, No. 9-10, pp. 1181-1192, 2010.

[97] A. W. Leissa, 'Vibration of Plates', Office of Technology Utilization, *National Aeronautics and Space Administration, Washington, DC*, 1969.